THE DYNAMICS OF NON-SPHERICAL PARTICLES. I. CONTROLLED GENERATION OF NON-SPHERICAL AEROSOLS AND METHODS FOR THEIR SIZE, CONCENTRATION AND ELECTRIC CHARGE MEASUREMENT

Isaiah Gallily

Hebrew University

Prepared for:

European Research Office

January 1974

UNCLASSIFIED
Security Classification

AD-783437

DOCUMENT CONTROL DATA - R & D

(Security classification of title, body of abstract and indexing annotation must be entered when the overall report is classified)

1. ORIGINATING ACTIVITY (Corporate author)	2a. REPORT SECURITY CLASSIFICATION
The Hebrew University of Jerusalem Jerusalem, Israel	Unclassified 2b. GROUP

3. REPORT TITLE

The Dynamics of Non-spherical Particles: I. Controlled Generation of Non-spherical Aerosols etc.

4. DESCRIPTIVE NOTES (Type of report and inclusive dates)

Final Technical Report

5. AUTHOR(S) (First name, middle initial, last name)

Dr. Isaiah Gallily

6. REPORT DATE	7a. TOTAL NO. OF PAGES	7b. NO. OF REFS
January 1974	46	63

8a. CONTRACT OR GRANT NO.	9a. ORIGINATOR'S REPORT NUMBER(S)
DAJA37-72-C-3875 b. PROJECT NO.	
c.	9b. OTHER REPORT NO(S) (Any other numbers that may be assigned this report) E-1531
d.	

10. DISTRIBUTION STATEMENT

Approved for public release; distribution unlimited.

11. SUPPLEMENTARY NOTES	12. SPONSORING MILITARY ACTIVITY
	USA R&D GP (EUR) Box 15, FPO N.Y. 09510

13. ABSTRACT

The typical features of the motion of a nonspherical aerosol particle are discussed, an overall aim concerning its behavior in systems of importance for human environment is stated, and a preliminary objective of studying methods for generation, size measurement, concentration determination and assessment of electric charge is set. Previous investigations in these lines are reviewed.

KEYWORDS: (U) Nonspherical aerosols; aerosols; charge measurement.

DD FORM 1 NOV 68 1473 REPLACES DD FORM 1473, 1 JAN 66, WHICH IS OBSOLETE FOR ARMY USE.

UNCLASSIFIED

THE DYNAMICS OF NONSPHERICAL PARTICLES

I. Controlled Generation of Nonspherical Aerosols and Methods for Their Size, Concentration and Electric Charge Measurement

Final Technical Report

by

Isaiah Gallily

January 1974

EUROPEAN RESEARCH OFFICE
United States Army
London W. 1, England

Contract Number DA JA 37-72-3875

The Hebrew University of Jerusalem, Jerusalem, Israel

TABLE OF CONTENTS

SUMMARY

The typical features of the motion of a nonspherical aerosol particle are discussed, an overall aim concerning its behaviour in systems of importance for human environment is stated and a preliminary objective of studying methods for generation, size measurement, determination of concentration and assessment of electric charge is set. Previous investigations in these lines are reviewed.

Starting with model shapes, there were produced by solution spray-drying almost perfect cubes or parallelpipeds and, by suspension gas atomization, cylindrical particles of glass fibers. The problem of the agglomerate size distribution obtained with the latter method of generation was studied experimentally whereby it has been found that the Poisson Distribution can not be assumed unquestionably. Dispersion of powders by air turbulence was treated theoretically and a computational investigation of the adhesional energy between two parallelpipeds at various mutual orientations begun. Preliminary results have been achieved.

The size parameters of the produced particles were determined in a scanning electron microscope by a recently developed photogrammetric method of observation which proved to sufficiently accurate.

A way of assessing the electric charge of a nonspherical particle is analyzed in view of the specificity of its motion and the relation to the principal translational resistances brought out. The resistance to slow motion of an ellipsoid at Knudsen numbers much smaller than unity has been computed by the numerical integration of the equations of Oberbeck, thus conferring an extra degree of freedom to the simulation of a particle.

The effect of Brownian rotation on the translation of an aerosol particle was discussed, a series of experiments in this line was set up, and results which confirmed the direct relationship between the averaging phenomenon and time achieved.

An apparatus for the determination of the principal resistances of a nonspherical particle at various Knudsen numbers has been constructed and a mathematical procedure for the elucidation of results developed.

I. INTRODUCTION

The dynamical behaviour of solid, nonspherical aerosol particles is very little known. In comparison with the relatively well-studied case of spherical liquid droplets, the motion of the former is much more complicated. Due to a lack of spherical symmetry (Fig. 1), these particles manifest a drift in a direction perpendicular to the acting force and, quite often, a coupled rotational translational movement. In addition, they undergo like their spherical counterparts stochastic Brownian motion which is caused by the incessant, fluctuating molecular bombardment of the dispersing medium.

The regular movement of solid particles can be formulated in terms of intrinsic tensors of translation, rotation, and coupling that are defined for the continuous regime, as an example, by (1)*

$$\vec{F}_{R,h} = -\mu \left(\vec{\vec{K}} \cdot \vec{v}_R + \vec{\vec{C}}_R \cdot \vec{\omega} \right) \qquad [1]$$

$$\vec{T}_{R,h} = -\mu \left(\vec{\vec{\Omega}} \cdot \vec{\omega} + \vec{\vec{C}}_R \cdot \vec{v}_R \right) , \qquad [2]$$

and by the equations of motion

$$m \, d\vec{v}_R / dt = \vec{F}_{R,h} + \sum_i \vec{F}_{ex,i} \qquad [3]$$

$$d\vec{H}_R / dt = \vec{T}_{R,h} + \sum_i \vec{T}_{ex,R,i} \, . \qquad [4]$$

The stochastic movement can be treated by Langevin type equations in which a time-dependent force $\vec{F}(t)$ or torque $\vec{T}(t)$ are included in the right-hand side of Eqs. [3] or [4], respectively (2).

The Brownian and regular rotation of a nonspherical particle affect its resistance to translation through the change in its orientation with respect to

---

* For nomenclature see Glossary

Fig. 1. Typical Photograph of Atmospheric Solid Particles; Coal Dust.
(Taken from "Particulate Clouds" by Green and Lane, Spon, 1964, Plate 3)

the acting external force and are quite detrimental for the phenomenon of aerosol collection by various obstacles (3).

The principal resistances to translation and rotation at low Reynolds numbers are a function of the particle's geometric shape and dimensions; however, very frequently the latter can not be given in terms of one or a few numbers as is the case with spherical droplets. To satisfy the essential need of size characterization, there has been adopted a variety of geometric and dynamical measures. The first group contains the "projected area diameter" d_p, which is derived from a circle whose area equals that of the particle's viewed silhouette (3); likewise, it includes the conceptually if not experimentally used "volumetric equivalent diameter" d_v that is related to a sphere of an identical volume. The second group is based on simulating significant features of particles' motion by the movement of simpler bodies. It consists of measures such as the Stokesian, d_s, or the aerodynamic diameter, d_a (4), which are the diameters of a solid sphere having a terminal velocity in the direction of gravity equal to that of the actual aerosol particle and the density of the latter or a density of unity, respectively. This group contains also the less known "rotationally equivalent ellipsoid" which has the same radii of gyration about its principal axes as those of the particle itself (5).

The problem of size specification of irregular particles is tied to the choice of successful models; however, since no one of the existing approachs does represent all the properties of the particle, it may be worthwhile to use a combination that will furnish a satisfactory description. Thus, every solid particle may be described by a set of numbers composed of the diameter of the "volumetric equivalent sphere", the three axes of a translationally equivalent and the three axes of a rotationally equivalent,ellipsoid.

Here one should note the specificity of nonspherical particles with regard to the action of electric forces. Again, as a result of a lack of spherical symmetry, the real or induced electric charges on the sufrace of these particles will be unevenly distributed and so, in the presence of external electric fields, solid aerosol particles would be subjected to additional torques.

II. STATEMENT OF AIM

Similarly to many aerosol studies, we set before ourselves the ultimate goal of determining the deposition efficiency in systems which are important for human environment. However, in view of the lack of basic knowledge on the dynamical behaviour of nonspherical particles, we prefered to use a methodical approach towards this aim. Thus, in the first stage of the investigation, we chose to deal with model aerosols and begin a study for:

1. Establishing methods of generation
2. Developing methods of three-dimensional size measurement
3. Assessing the electric charge of the particles.

The electric charge can be determined by measuring the motion of a particle in a combined gravitational — electric field and utilizing thereafter the terminal state equations (6)

$$\vec{F}_g + \vec{F}_{el} = \mu \left(\vec{\vec{K}} \cdot \vec{v}_t + \vec{\vec{C}}_R \cdot \vec{\omega} \right) \qquad [5]$$

$$\vec{T}_g + \vec{T}_{el,R} = \mu \left(\vec{\vec{\Omega}}_R \cdot \vec{\omega} + \vec{\vec{C}}_R \cdot \vec{v}_R \right) \qquad [6]$$

which turn in the case of spin-free ($\vec{\omega} = \vec{0}$) symmetric enough ($\vec{\vec{C}}_R = \vec{\vec{0}}$) shapes into

$$m\vec{g} + q\vec{E} = \mu \vec{\vec{K}} \cdot \vec{v}_R \qquad [7]$$

In the latter case it is essential to know the translation tensor and hence, one has to study preliminarily:

a. The principal translational resistances of the particles at various Knudsen numbers, Kn

b. The effect of the rotational Brownian motion on the real trajectory.

The last objective seemed to us of primary importance as it reflected the statistical nature of a particle's movement which stems from the random change of its orientation (Chap VII b).

It ought to be remarked with regard to the general use of a model that, though simplifying matters enormously, it still leaves one with the question of which properties are represented and at what accuracy.

III. PREVIOUS STUDIES

a. Generation of Aerosols

The formation of solid aerosols for technical and research purposes has been carried out by the following methods:

1. Spray-drying of solutions and suspensions (7, 8)
2. Powder dispersion by a turbulent gas (9)
3. Condensation of vapours by thermal or pyrotechnic means (10, 11).

The final product of these techniques is an aerosol of primary or agglomerate particles whose initial size distribution depends on the mechanism of generation and on the immediate coagulation thereafter.

Fundamentally, the processes of formation have been studied solely for solution spray-drying (12, 13) and vapour condensation (14). No direct investigation has been reported on production of agglomerates during suspension spray-drying or in powder dispersion by air.

b. Size Measurement

The size determination of nonspherical particles has been performed by methods based on geometric measures and operationally convenient concepts. The most widely used among the first is the "projected area diameter" which is now determined also with some new instrumentation (15, 16). Among the second is the "aerodynamic diameter" which can be measured with Stober's spectrometer and similar apparati (17, 18) or a suitable wind tunnel (19). The "projected area diameter" depends on the orientation of the measured particle at the surface of collection and so does not constitute an instrinsic property (20, 21, 22). Lately, a photogrammetric way of viewing each particle from three directions of sight and calculating its dimensions has been proposed and checked (20).

The aerodynamic diameter is founded on the comparison between the vertical component of the overall velocity of fall and that of a sphere. Thus, it does not take into account the full complexity of the motion of a nonspherical particle nor its statistical nature (Chap. VII b). Due to the very nature of the movement, it may happen that identical particles would be represented by various aerodynamic diameters, which shows one of the inherent limitations in the modeling procedure.

c. Number Concentration

The number concentration of solid aerosols has been measured by :

1. Collection of particles from a known volume of gas with the aid of suitable filters (23, 24) or impactors (25, 26) and a subsequent counting
2. Observation of light signals produced by individual particles that stream at a measured rate through some sensing sub-space, as in the Royco Instruments (27) and the Derjagin-Vlasenko flow tube (28)
3. Dark-field photography of the particles contained in a well defined volume (29).

d. Electric Charge Distribution

The electric charge of nonspherical aerosols has been determined mostly by :

1. Measuring the velocity of individual particles in a uniform electric field (30)
2. Ascertaining the mobility and some convenient size measure of particles which pass in a laminar flow through a suitable electric condenser.

Here, again, there has been paid no attention to the aforementioned complexity of motion and what has been deduced from these two methods has been only the Stokesian or aerodynamic diameter.

IV. MODELS AND METHODS OF GENERATION

a. Spray-drying of Solutions

To produce particles of a simple shape we experimented first with 2.44 M aqueous solutions of sodium chloride. The apparatus employed consisted of a Dautrebande nebulizer (31) and a 210 x 107 x 100 cm evaporation chamber (Fig. 2) in which the spray-drying was performed. Using this technique one is confronted frequently with clogging of nozzles by a dried-up crust of salt; however, we overcame this difficulty by incorporating in the sprayer air line a train of wash-bottle humidifiers (32).

The dry particles were sampled with the aid of a thermal precipitator (Casella, London) in which special arrangement was made to accommodate stubs of a scanning electron microscope (Fig. 3), and were observed thereafter in the latter. The collecting surfaces were prepared by cementing to the stubs thin coverglasses so as to get a smooth substrate. The produced particles were found to be almost perfect cubes or parallelpipeds (Fig. 4), which was not self-evident at all. In general, the shape of the dry residue from an evaporating droplet would depend on an interplay between the rate of diffusion of the solvent into the surrounding gas and the rate with which the solute molecules adjust themselves on the firstly formed solid nucleous or nuclei. Thus, under conditions of high supersaturation, one can get from the same sodium chloride material almost ideal spheres (33).

The initial size distribution of the particles is related to that of the primary solution-droplets and the concentration of the salt by

$$f(s) = h(r) \qquad [8]$$

where $r = A_1 (s/c_1^{4/3})$ and A_1 is a constant of the order of unity. One should note though that the density of the residues is not necessarily equal to the density of the bulk crystal and so has to be checked.

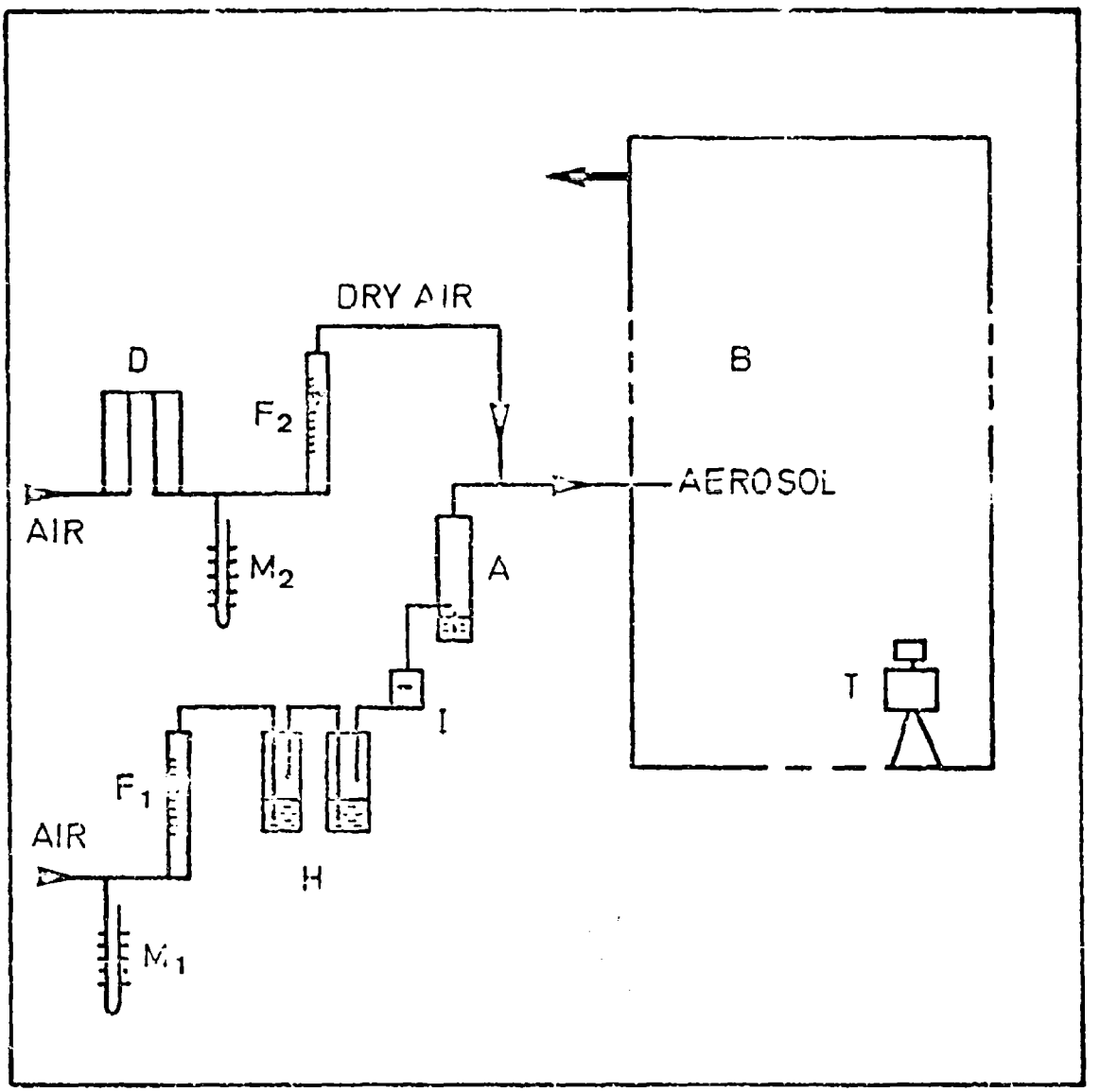

Fig. 2. Block Diagram of the Spray-drying Apparatus Used for Solutions.
A - Nebulizer, B - Evaporation Chamber, D - Driers,
F_1, F_2 - Flowmeters, H - Humidifiers, I - Impactor,
M_1, M_2 - Manometers, T - Thermal Precipitator.

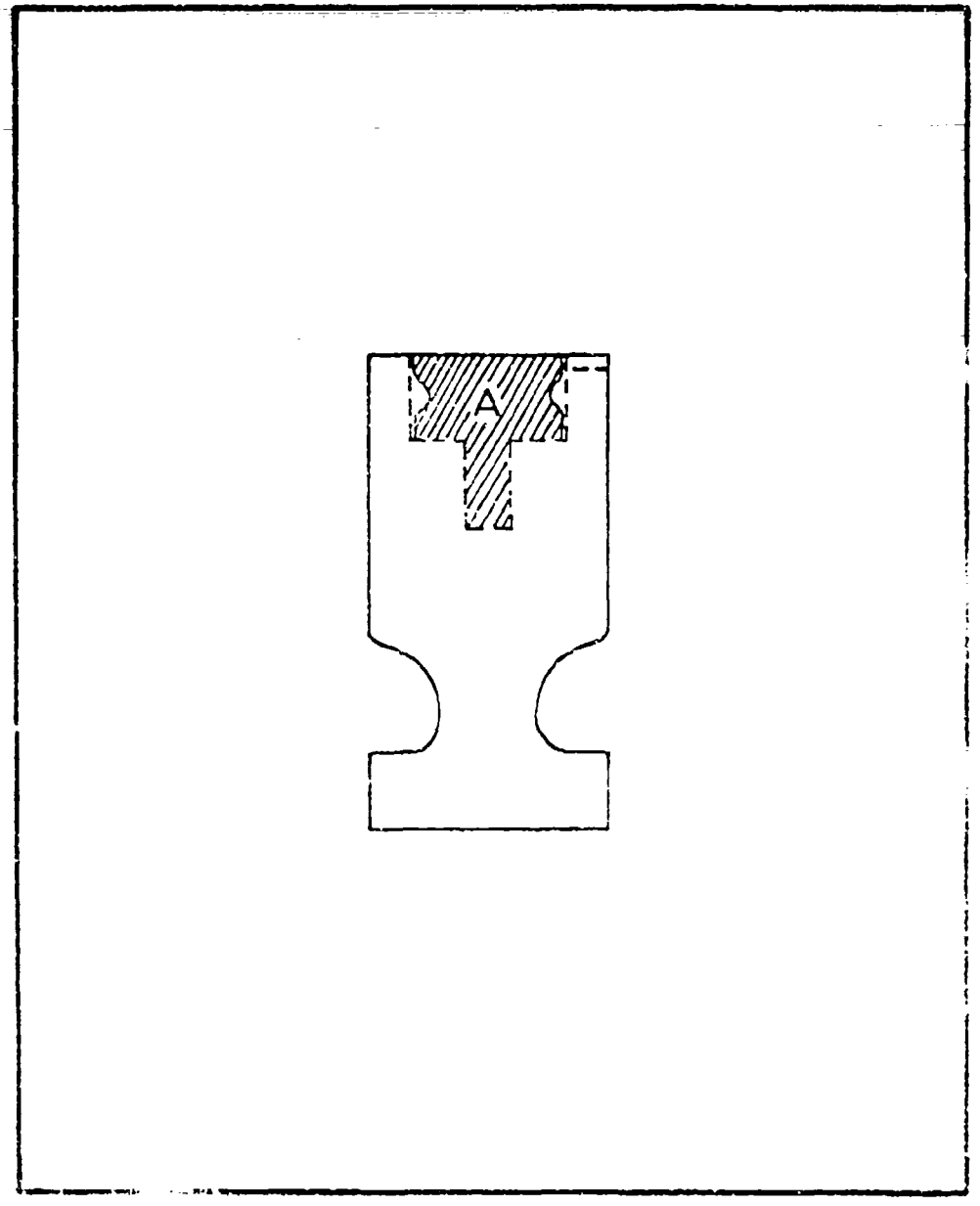

Fig .. Thermal Precipitator Holder for a Stub of a Scanning Electron Microscope (Schematical).

A - Stub.

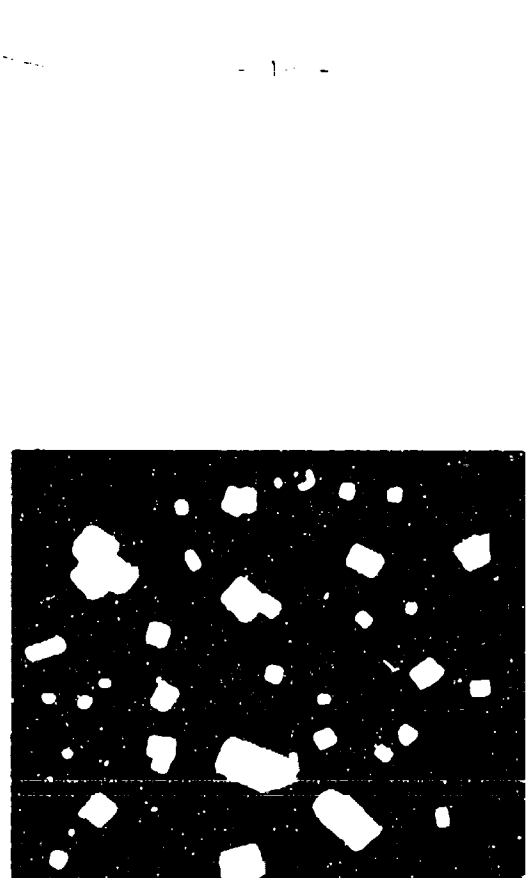

Fig. 4. Sodium Chloride Particles (Gold Shadowed, Total Magnification - 8333)

b. Spray-drying of Suspensions

This method was employed with a suspension of glass fibers that was prepared by mashing a filter mat (Whatman, GF/C Glass Fiber Paper) soaked in demineralized water. The suspension (1.10 g/l) was spray-dried in an apparatus (Fig. 5) consisting of a modified Dautrebande Sprayer A equipped with an adjustable impactor (34), and a drying column B. The formed particles were sampled by gravitational sedimentation on stubs prepared by the technique mentioned above, and then observed in the scanning electron microscope. The particles were seen to be cylindrical in shape (Fig. 6).

Comparing the typical size of the cylinders with that of the suspension droplets, there arose the question of the physical accommodation of the large fibers within the latter. It may be interesting to inquire into the problem by a suitable series of experiments, but this was postponed for the future.

Another point to investigate was the agglomeration of primary solid particles which was due to the presence of more than one "primary" in an evaporating droplet.

(i) Check of the Poisson Distribution

Up to now it has been assumed that the probability of a suspension-droplet to contain n primary particles is governed by the Poisson Distribution (35 - 7)

$$f(n, \bar{n})_t = e^{-\bar{n}} \cdot \bar{n}^{n} / n! \quad , \qquad [9]$$

where $\bar{n}$, the first moment (- the arithmetic average) of the number concentration, is given by

$$\bar{n} = (4/3)\,\pi\, r^3\, Q \quad . \qquad [10]$$

This has been also the guiding formula for performing the necessary dilution of the bulk suspension in order to obtain pedominantly single particles.

The assumption of a Poisson Distribution is mathematical in nature; thus, as the physics of liquid disruption and the distribution of "primaries"

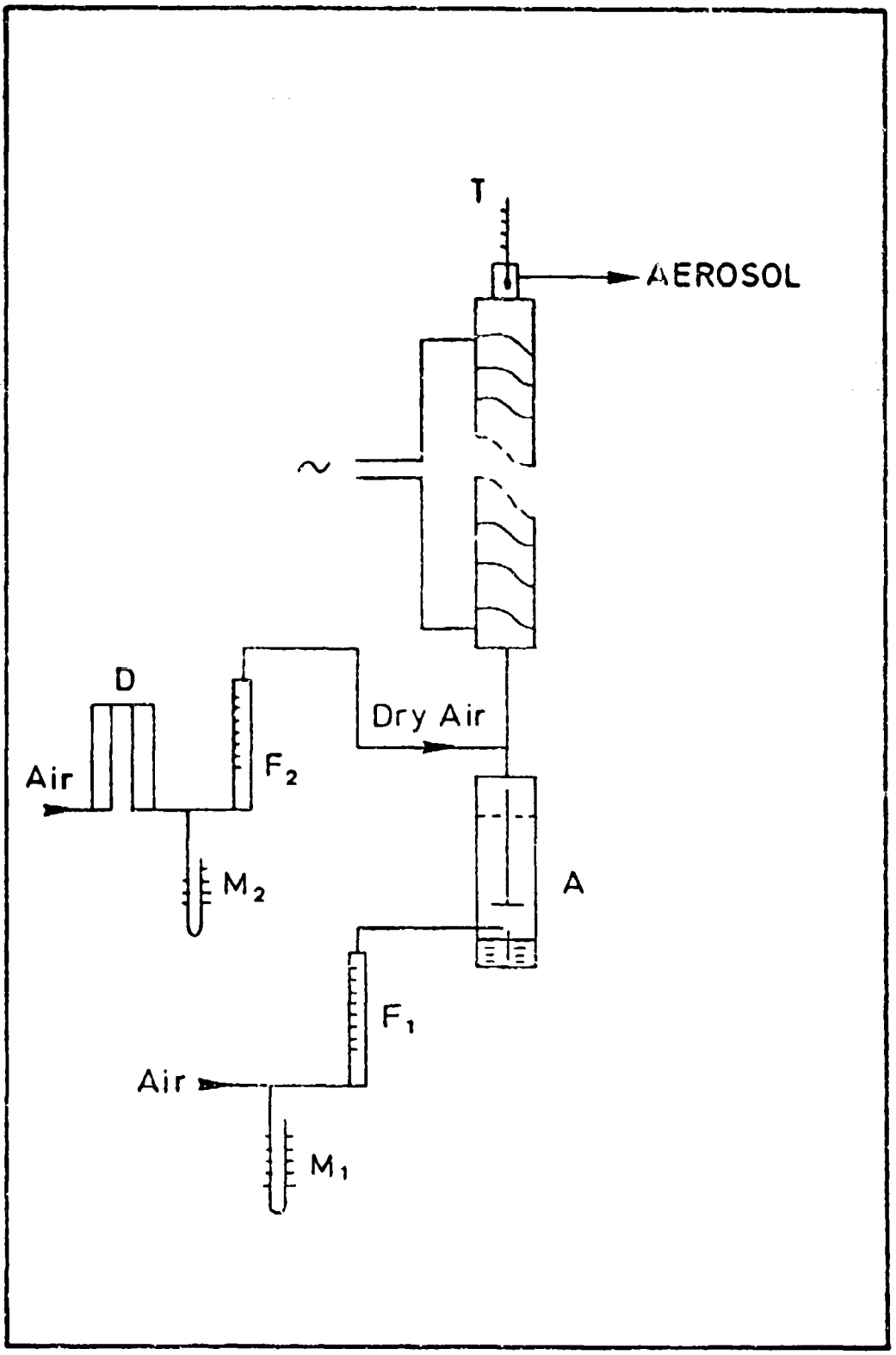

Fig. 5. Block Diagram of the Spray-drying Appartus Used for Suspensions.

D - Driers, F_1, F_2 - Flowmeters,

M_1M_2 - Manometers, T - Thermometer.

Fig. 6. Glass Fiber Particles (Gold Shadowed, Total Magnification - 3666)

within the droplets could conform to different laws, we thought it worthwhile to check the point experimentally.

Experimental

The experiments towards this aim consisted of spraying an aqueous suspension of Polystyrene Latex particles (Dow Chemical Company, Biophysics Department, Midland, Michigan) in a saturated humid atmosphere, and then collecting the sedimenting droplets on a mixture of Dioctylphthalate (DOP)-Diethylphthalate (DEP) which embodied them and prevented their evaporation (38). The collected droplets were photographed through a microscope, the radii of their images measured, and the number of latex particles in each one of them counted.

The apparatus employed in the investigation (Fig. 7) was composed of a spinning top instrument A (Reaserch Engineers, London) which was enclosed within a chamber humidified by a hot water bath B, a hanging-drop microscopic slide C that contained the DOP-DEP, and a burette D from which an extra thin layer of the mixture was applied after collection to effect a complete separation from air. The latex particles used were characterized by a diameter of 1.305 um and a standard deviation of 0.0158 um. The original suspension (10% v/v of solids) was diluted 2500-fold with demineralized water. To ensure that the photographed droplets would remain spherical we adjusted the density of the DOP-DEP to be a little smaller than that of the latex emulsion so that each droplet settled down to the bottom in a time much greater than that needed for a measurement. It has been found that using unclean microscopic slides is advantageous as each suspension droplet that sediments spreads out into a non-circular contour and can be discerned.

A typical photograph of a droplet immersed in a DOP-DEP mixture is brought out in Fig. 8. The radii of the droplets used ranged between 15 to 50 μm and the average concentration $\bar{n}$, deduced from actual counting, was found to be invariable over the period of the whole series of experiments.

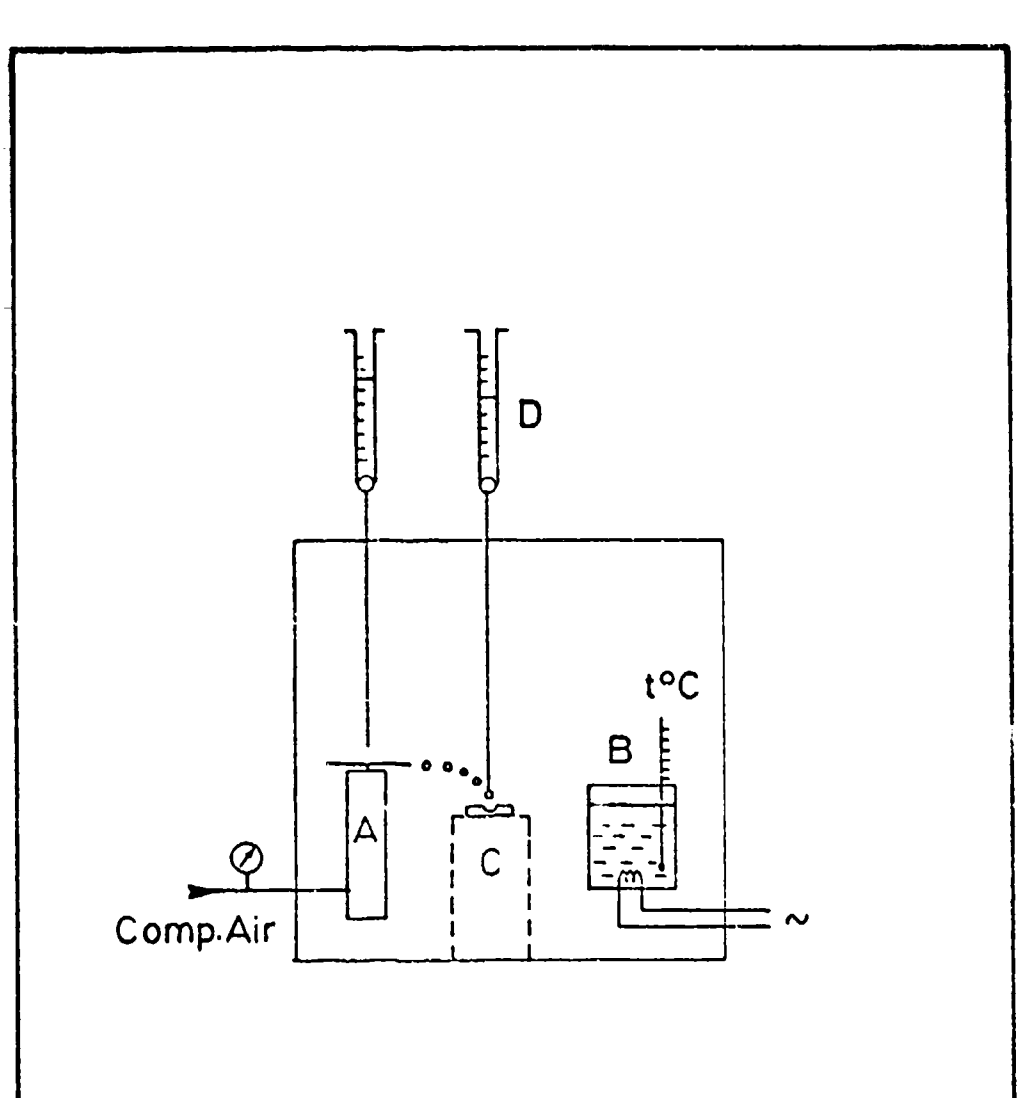

Fig. 7. Block Diagram of the Apparatus for Spraying of Suspensions.

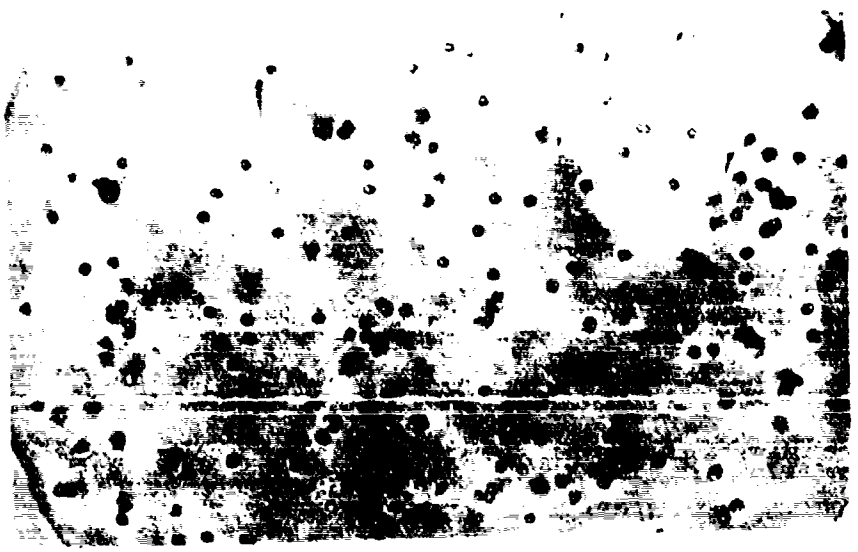

Fig. 8. Suspension-Droplet Immersed in a DOP-DEP Mixture.

As an extra caution, the fraction of agglomerates within the bulk suspension was checked and seen to be negligible.

Results

The results from particle counts were grouped in the form of a cumulative frequency $F(n)$ expressing the fraction of droplets which contained n primary particles.

$$F(n) = \sum_{r=r_1}^{r=r_2} f(n, \bar{n})\, g(r) \qquad [11]$$

A comparison between the found and expected frequencies is given in Tables 1, 2, and 4. To check the fitness between the experimental results and the Poissonian Distribution we applied the χ^2 -test whereby a value of 10.1 for Experiment Series 1 and 129.8 for Experiment Series 2 was obtained. As the number of the observed suspension-droplets was inevitably limited, we normalized both the experimental and the theoretical cumulative frequencies by dividing each one of them by the sum

$$F(n)_{nc} = \sum_{n=0}^{n=3} F(n) \qquad [12]$$

which seemed reasonable since essentially the maximal number of checked "primaries" has been 3. The processed data is brought out in Tables 3 and 5, from which the pertinent χ^2 values were deduced to be 5.9 and 111.9, respectively. The results are shown also in Figs. 9 and 10. The radii of the suspension-droplets pertaining to Experiment Series 1 were measured directly under the microscope with an accuracy of about 10 %, whereas the determination of the image-radii was carried out with an accuracy of about 2 %.

Number of Droplets Checked	n / d(μm)		0	1	2	3	4	g(r)
26	16	$f(n,\bar{n})_e$	0.85	0.15	0.00	0.00	0.00	0.086
		$f(n,\bar{n})_t$	0.94	0.05	0.01	0.00	0.00	
28	20	$f(n,\bar{n})_e$	0.50	0.36	0.10	0.04	0.00	0.092
		$f(n,\bar{n})_t$	0.89	0.10	0.01	0.00	0.00	
80	24	$f(n,\bar{n})_e$	0.76	0.16	0.07	0.00	0.00	0.264
		$f(n,\bar{n})_t$	0.82	0.16	0.016	0.001	0.00	
28	28	$f(n,\bar{n})_e$	0.82	0.18	0.00	0.00	0.00	0.092
		$f(n,\bar{n})_t$	0.73	0.23	0.03	0.004	0.00	
78	32	$f(n,\bar{n})_e$	0.69	0.24	0.04	0.03	0.00	0.257
		$f(n,\bar{n})_t$	0.629	0.291	0.067	0.010	0.001	
20	36	$f(n,\bar{n})_e$	0.45	0.35	0.10	0.05	0.00	0.066
		$f(n,\bar{n})_t$	0.52	0.34	0.11	0.02	0.004	
25	40	$f(n,\bar{n})_e$	0.36	0.44	0.16	0.00	0.04	0.082
		$f(n,\bar{n})_t$	0.40	0.37	0.16	0.05	0.01	
8	44	$f(n,\bar{n})_e$	0.37	0.12	0.37	0.00	0.12	0.026
		$f(n,\bar{n})_t$	0.30	0.36	0.22	0.09	0.03	
10	48	$f(n,\bar{n})_e$	0.50	0.20	0.10	0.20	0.00	0.033
		$f(n,\bar{n})_t$	0.21	0.33	0.26	0.13	0.05	

Table 1: Comparison between Differencial Frequencies of "Primary" Occurance. Experiment Series 1 ($Q_o = 2.7 \times 10^7$ particles / cm^3; total number of checked droplets — 303)

n	$F(n)_e$	$F(n)_t$
0	0.66	0.69
1	0.24	0.20
2	0.07	0.06
3	0.02	0.01
4	0.007	0.002

Table 2: Comparison between Found and Expected Cumulative Frequencels of "Primary" Occurance. Experiment Series 1

($Q = 2.7 \times 10^7$ particles / cm^3;
total number of checked droplets — 303)

n	$F(n)_{e,no}$	$F(n)_{t,no}$
0	0.67	0.72
1	0.24	0.21
2	0.07	0.06
3	0.02	0.01

Table 3: Comparison between Found and Expected Normalized Cumulative Frequenceis of "Primary" Occurance.
Experiment Series 1

($Q = 2.7 \times 10^7$ particles / cm^3;
total number of checked droplets — 303)

n	$F(n)_e$		$F(n)_t$
	200 droplets	439 droplets	
0	0.61	0.58	0.54
1	0.26	0.26	0.15
2	0.07	0.10	0.04
3	0.03	0.04	0.01
4	0.00	0.01	0.002

Table 4: Comparison between Found and Expected Cumulative Frequencies of "Primary" Occurance.
Experiment Series 2
($Q = 2.69 \times 10^7$ particles / cm^3 ;
total number of checked droplets — 439)

n	$F(n)_{e,\,no}$	$F(n)_{t,\,no}$
0	0.59	0.73
1	0.26	0.20
2	0.10	0.05
3	0.05	0.01

Table 5: Comparison between Found and Expected Normalized Cumulative Frequencies of "Primary" Occurance. Experiment Series 2

($Q = 2.69 \times 10^7$ particles / cm^3 ;
total number of checked droplets - 439)

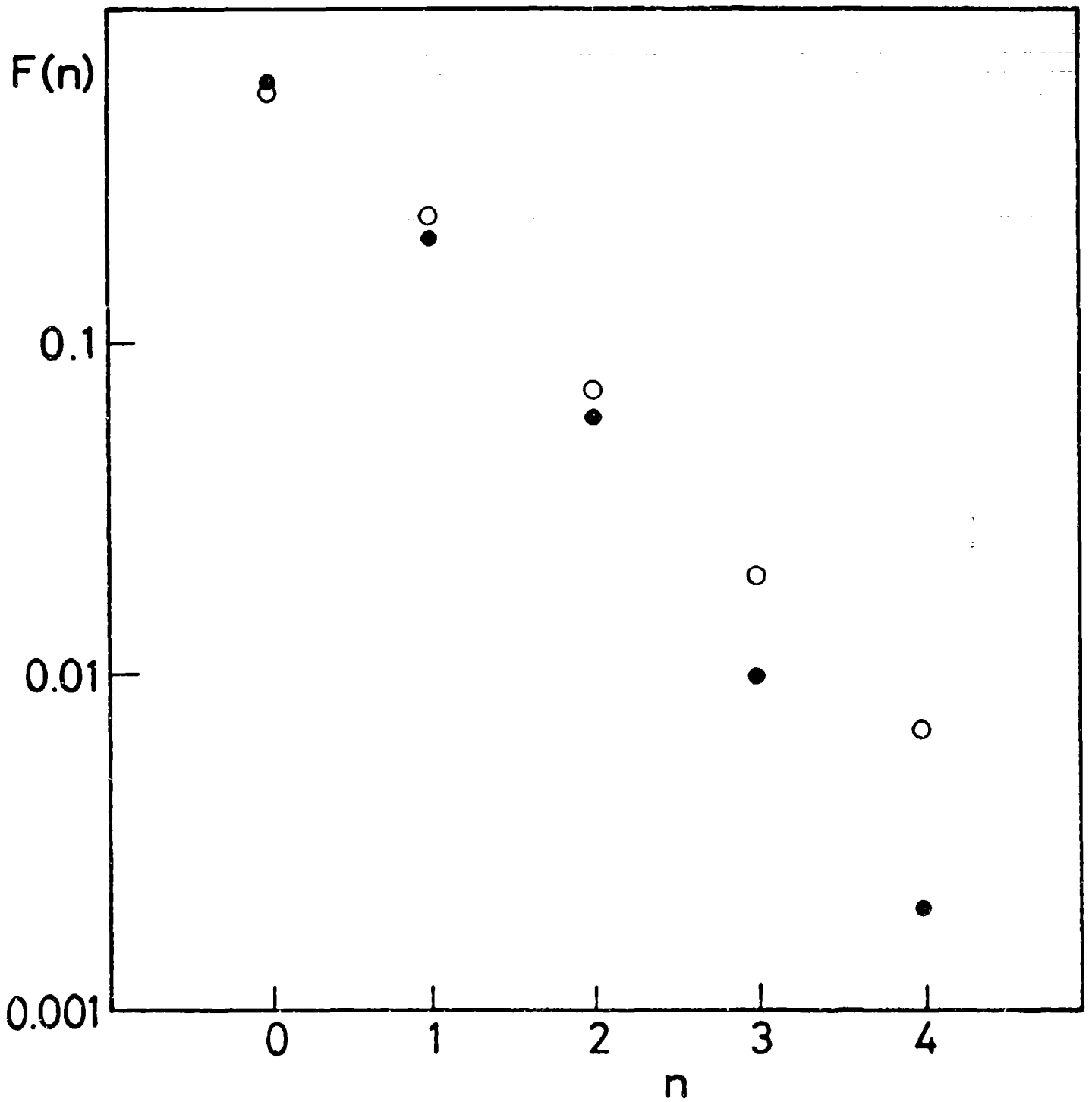

Fig. 9. Cumulative Distribution of Agglomerate Size .
(Experiment Series 1, Table 2).
○ - Experimental, ● - Theoretical

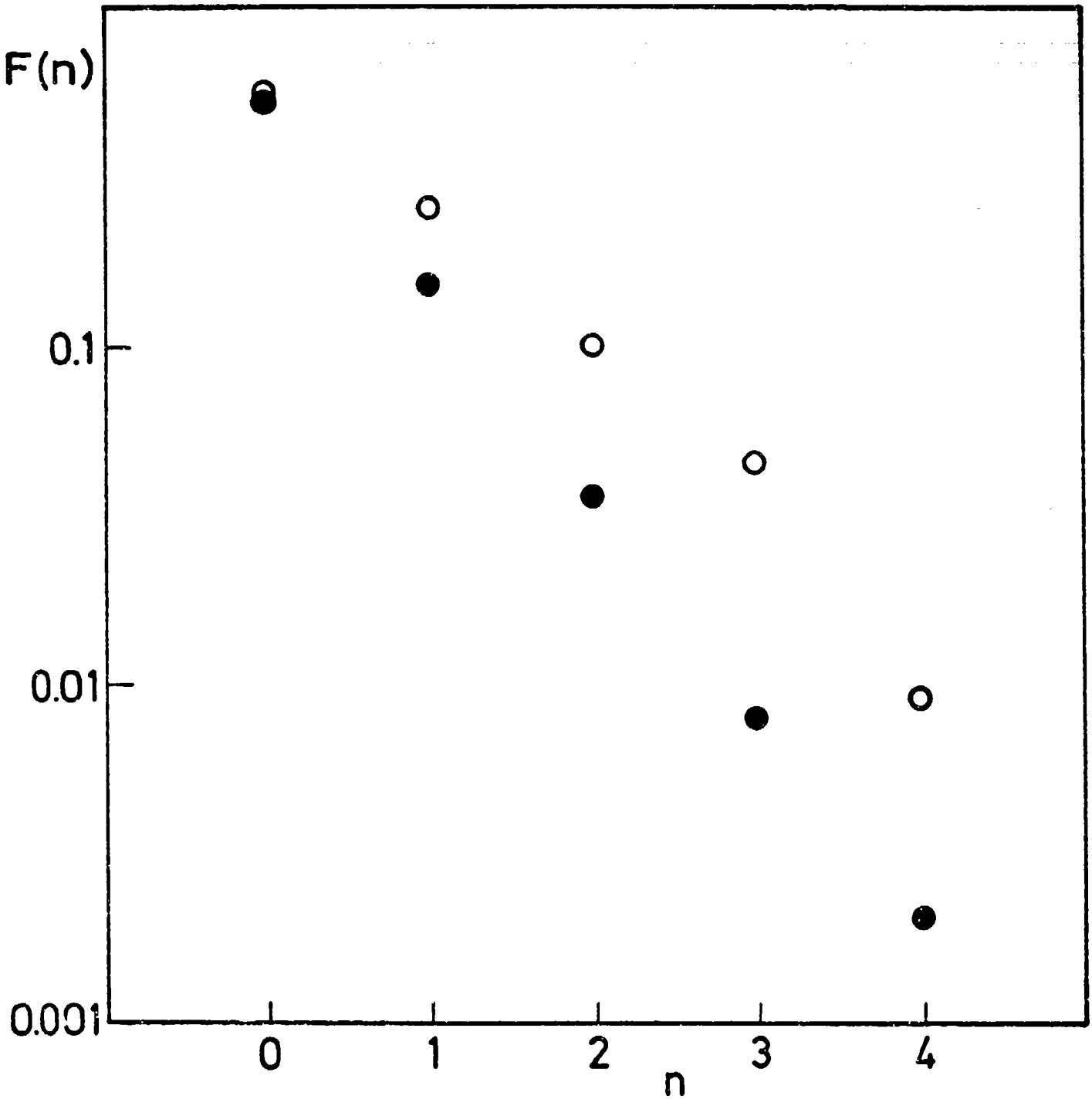

Fig. 10. Cummulative Distribution of Agglomerate Size .
(Experiment Series 2, Table 4, 439 Droplets)
o - Experimental, • - Theor

Discussion

The comparison between the experimental results and the theoretical expectations points out that the distribution of agglomerate sizes in our case of dispersion from a spinning top is significantly not Poissonian. This is in discord with the study of Raabe (37). One should note that in general it is not safe to match distributions according to their tails; so, any applicability examination has to be regarded only as a test for a representative mathematical formula.

The process of "primary" distribution within the droplets depends probably on the mechanism of suspension disruption. It surely needs further investigation especially to clarify the influence of particle shape. The immediate conclusion,however, is that considerations of pre-dilution based on the Poissonian Distribution can not be relied upon unquestionably and need be checked in every case.

c. Dispersion of Powders by Air Turbulence

In spite of its extensive use for a long time the dispersion of a powder by turbulent gas has not been treated in a quantitative way. Thus, we thought it worthwhile to try a rough analysis of the problem.

If one pays attention to a powder-aggregate that is lifted into air by turbulence and is subjected to the mutually opposing action of fluctuating energy of motion (Fig. 11 a) and adhesion between neighbouring "primaries", then one can formally write for the equilibrium dynamic state (39)

$$\overline{E_T(\vec{\ell}_{eff.})} = E_A \quad . \qquad [13]$$

The average fluctuating energy within an agitated aerosol in which local isotropy is assumed, for example, can be expressed by

$$\overline{E_T(\vec{\ell}_{eff.})} \propto s|\vec{\ell}_{eff}| \; \overline{v^2(\vec{\ell}_{eff.})} \qquad [14]$$

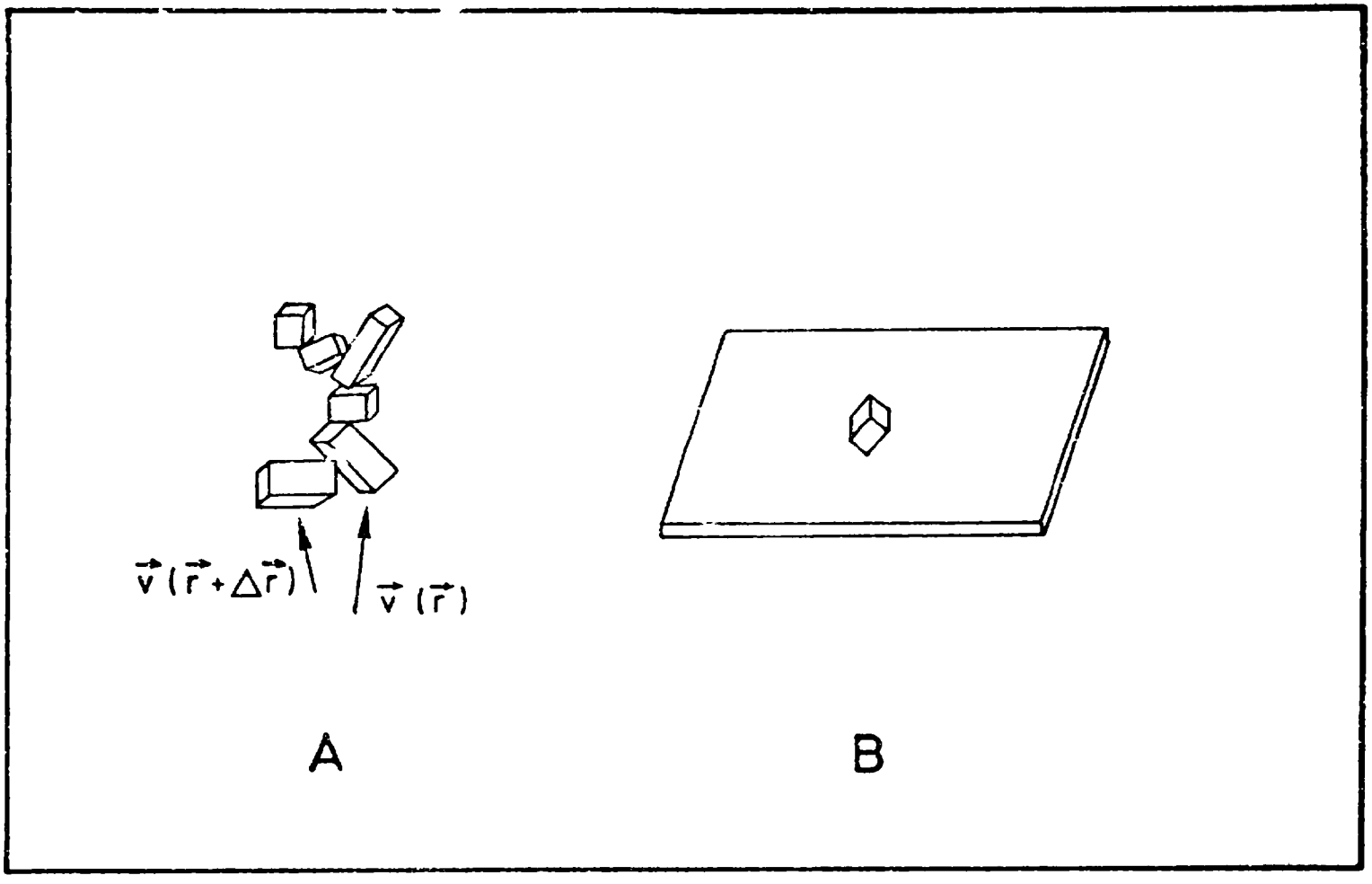

Fig. 11. A. Schematic Aggregate in a Turbulent Medium.
B. Parallelpiped Particle in Conact with a Solid Plane.

where $\overline{\vec{v}^2(\vec{\ell}_{eff.})}$ is given in

$$\overline{\vec{v}^2(\vec{\ell}_{eff.})} = C_1 \epsilon^{2/3} |\vec{\ell}_{eff.}|^{2/3} \qquad [15]$$

for the case of $\eta \ll |\vec{\ell}_{eff.}| \ll L_1$

and in

$$\overline{\vec{v}^2(\vec{\ell}_{eff.})} = C_2 \epsilon \vec{\ell}_{eff.}^{\,2} / (\mu/\rho) \qquad [16]$$

for the case of $|\vec{\ell}_{eff.}| \ll \eta$, η being the scale of eddies of Reynolds number 1 possesing maximum energy-dissipating properties. The energy of adhesion, on the other hand, has been calculated under the assumption of a Lennard-Jones, seventh power law for the cases of:

a. Two spheres, or a sphere and a plane as an asymptotic instance (40, 41)
b. Two parallel plates whose area is large compared to their separation (40)
c. Two discs of infinite thinness (42)
d. Two parallelpipeds that are oriented parallel to each other (43).

The case of the parallelpipeds was further treated by us in a way wh... the mutual orientation was allowed to vary, which was thought to be signifi... also for problems of sticking of particles that impinge on solid planes at an arbitrary angle (44) (Fig. 11b). In Vold's study (43), the potential integral

$$E_a = -\int_{V_1, V_2} (q_1^2 \lambda_1 / r_c^6)\, d\zeta_1\, d\zeta_2 \qquad [17]$$

is written in cartesian coordinates as

$$E_a = -q_1^2 \lambda_1^2 \iiint\!\!\iiint \frac{dx''\,dy''\,dz''\,du''\,dv''\,dw''}{[(x''-u'')^2+(y''-v'')^2+(z''-w'')^2]^3} \qquad [18]$$

wherefrom she gets after two integrations

$$E_a = -(q_1^2 \lambda_1/8) \iiint dx'' dy'' du'' dv'' \left[< \frac{1}{R^2 + (z'' - w'')^2 / R^2} \right.$$

$$\left. - \frac{3(z''-w'')}{R^5} \tan^{-1}\left(\frac{x''-u''}{R} \right) \right] \qquad [19]$$

in which $R^2 = (x''-u'')^2 + (y''-v'')^2$.

For the instance of two parallelpipeds having one face in the same plane (Fig. 12), and for identical particles of length ℓ, she obtains (43)

$$E_a = -(q_1^2 \lambda_1/4) \iiint dx'' dy'' du'' dv'' \left[(1/R^4) \right.$$

$$\left. - \frac{1}{(R^2+\ell^2) R^2} + \frac{3\ell}{R^5} \tan^{-1} \frac{\ell}{R} \right] \qquad [20]$$

that was expanded in powers of $R/\ell < 1$ to give

$$E_a = -(q_1^2 \lambda_1/4) \iiint dx'' dy'' du'' dv'' \left[(3\pi \ell / 5 R^5) \right.$$

$$\left. - (2/R^4) + \sum_{n=0}^{\infty} (-1)^n \frac{2(n+1) R^{2n}}{(2n+5) \ell^{2n+4}} \right] . \qquad [21]$$

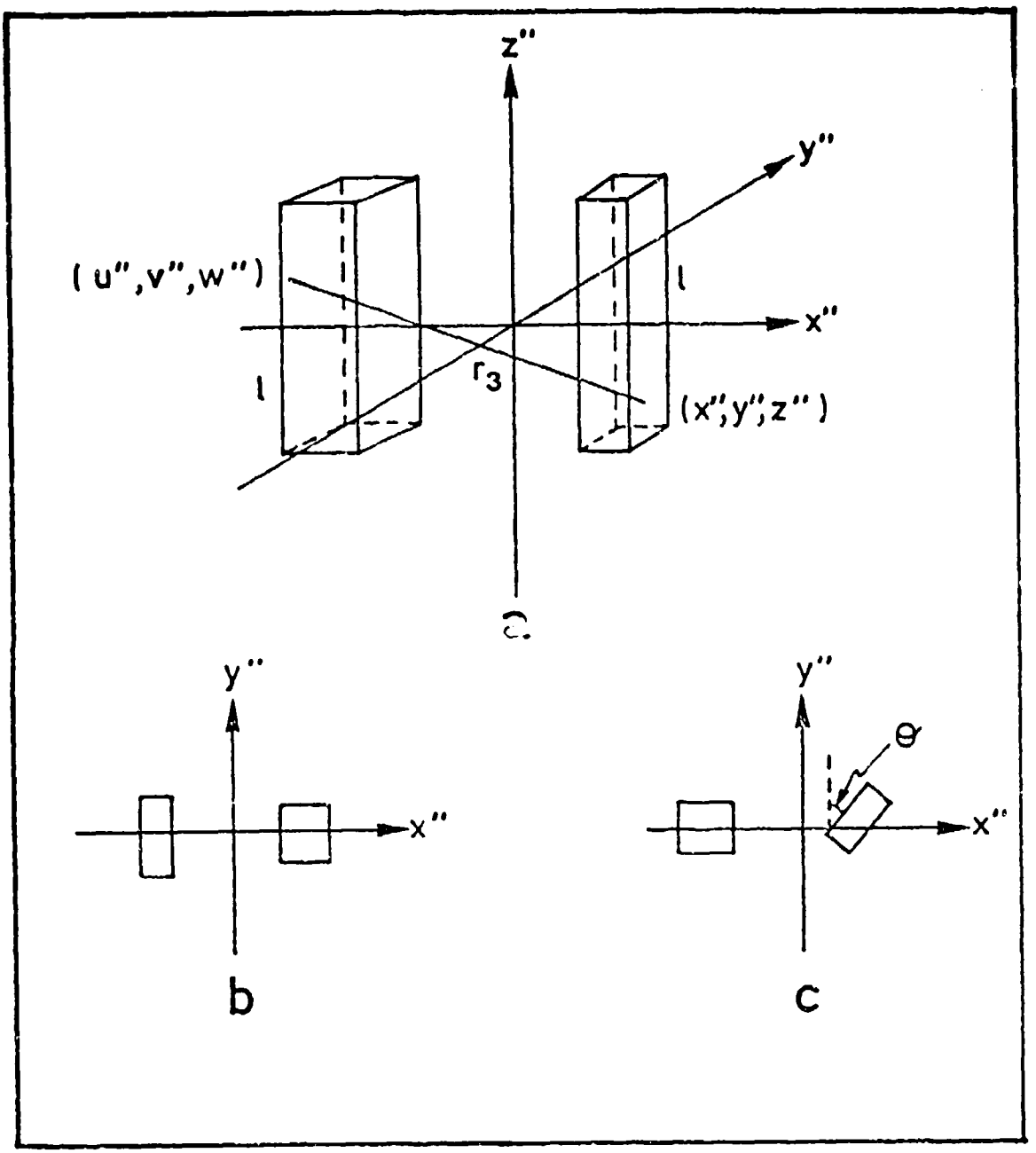

Fig. 12. Two Identical Parallelpiped Particles in Various Mutual Orientations.

Here we extended the mathematical treatment to include mutual orientation of $0 \leq \theta \leq \pi/2$ (fig. 12 c). A part of the results for the adhesional energy vs. θ is presented in Fig. 13 but studies in this line are still in progress.

(i) Dispersion of a Dry Power (Experimental)

Dispersion of our glass fiber powder was finally performed by a vigorous shaking of the dry material and application of an air stream to carry over the floating particles. The glass powder was prepared by subjecting the commercially available mats to a cutting action of a 2 blade, 3 cm long flat propeller (ESGE, 100 W blender) at 10000 rpm for 3 minutes.

V. SIZE DETERMINATION

Naturally, the true size of a nonspherical particle would be specified by the internally-based coordinates of its surface points. This is a difficult task that can be accomplished essentially in a number of ways (5, 20). The method adopted by us was photogrammetric in the sense that a three dimensional pattern was infered from information of a two dimensional space. Every particle was viewed through an electro-optical instrument from three directions of sight (Fig. 14), the $x_{i(j)}$, $z_{i(j)}$ coordinates of the images noted and the data processed according to the equations (45)

$$x_{i,j} = (1/2 \cos \sigma_1)[(x_i / M_i) + (x_j / M_j)] = X_{i,j} , \quad [22]$$

$$y_{i,j} = (1/2 \sin \sigma_1)[(x_j / M_j) - (x_i / M_i)] = Y_{i,j} , \quad [23]$$

$$z_{i,j} = z_i / M_i = z_j / M_j = Z_{i,j} , \quad [24]$$

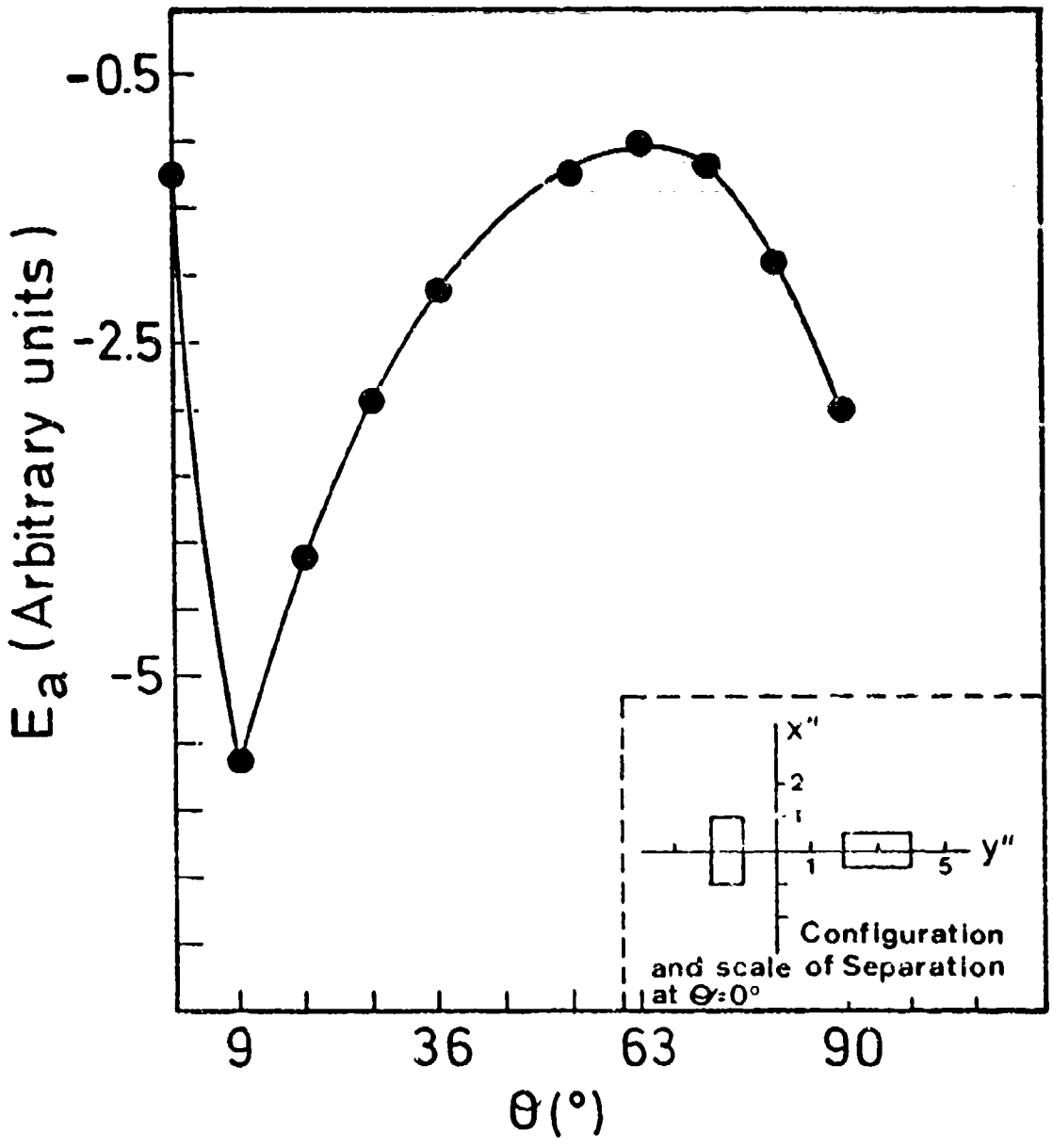

Fig. 13. Energy of Adhesion between two Parallelpiped Particles vs. Angle of Orientation (Arbitrary Units).

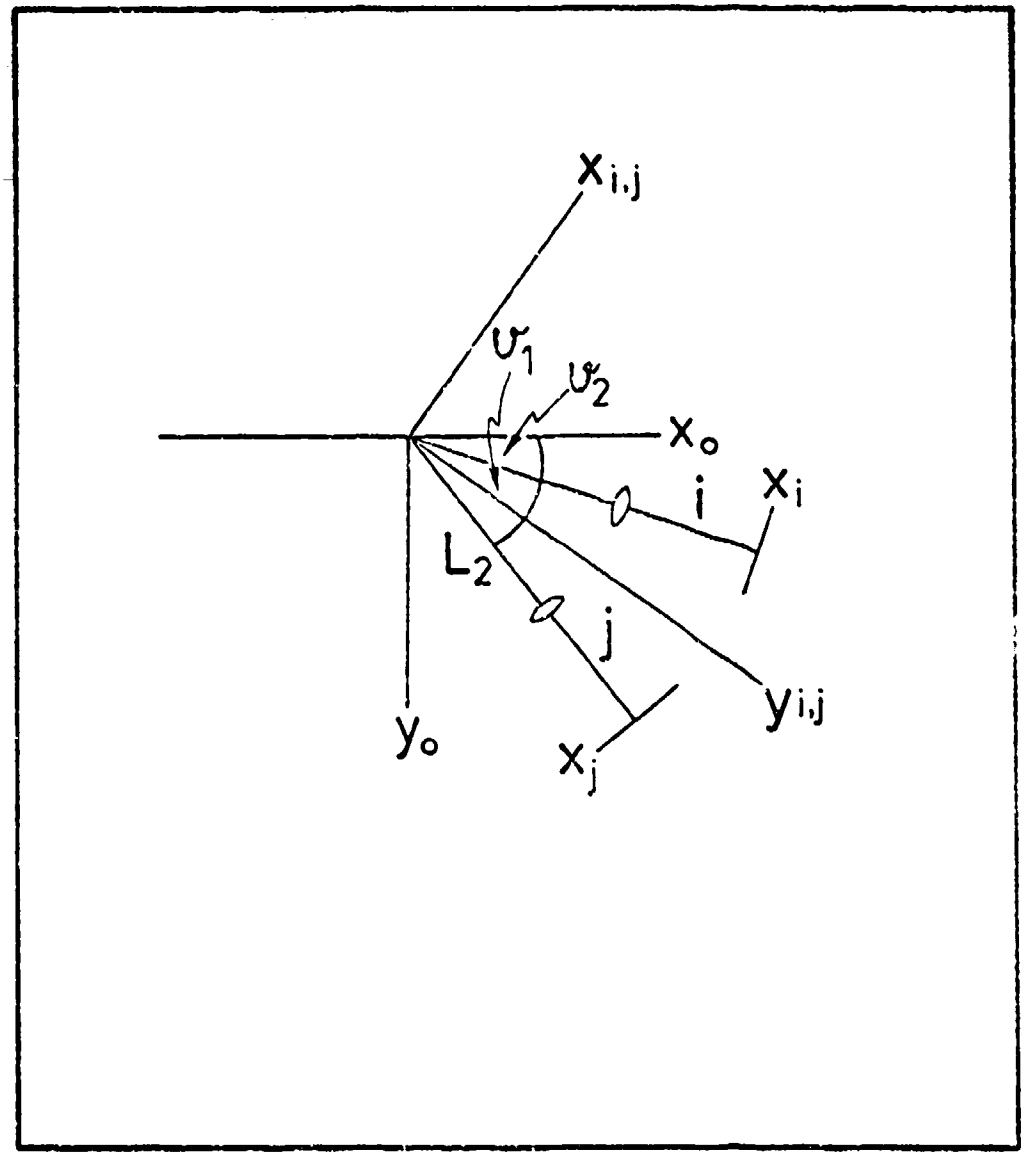

Fig. 14. Coordinate System Used in Photogrammetric Method of Size Determination.

$$x_0 = X_{i,j} \cos\beta + Y_{i,j} \sin\beta \quad , \qquad [25]$$

$$y_0 = -X_{i,j} \sin\beta + Y_{i,j} \cos\beta \qquad [26]$$

and $$z_0 = Z_{i,j} \quad , \qquad [27]$$

where $\beta = (\pi/2) - (\sigma_1 + \sigma_2)$, $i = 1, 2$ and $j = i + 1$.

In our study we used the Hebrew University Scanning Electron Microscope (Stereoscan Mk IV, Cambridge, England) in which the secondary emission mode was employed. Limiting ourselves to cylindrical particles (Fig. 6), we had a relatively simple object of determining only two parameters, viz. the length L and the diameter C. The particles were collected on glass covered stubs, shadowed with gold up to a thickness of a couple of hundred Angstroms, and observed from 0^o, 20^o, and 40^o. In the actual instrumental technique, the angle of sight was changed by small increments while refocusing constantly on the image. Particle length was calculated by the equation

$$L = (X_{i,j}^2 + Y_{i,j}^2 + Z_{i,j}^2)^{1/2} = (1/2)[4(x_i/M_i)^2$$

$$+ A_2\langle (x_i/M_i)^2 + (x_j/M_j)^2 \rangle - 2B_1 x_i x_j / M_i M_j]^{1/2} \qquad [28]$$

where $A_1 = [(1/\sin^2\sigma_1) + (1/\cos^2\sigma_1)]$

and $B_1 = [(1/\sin^2\sigma_1) - (1/\cos^2\sigma_1)]$.

The diameter of the fibers was deduced from the (unvaried) projection $C_{i(j)}$ perpendicular to the direction of length,

$$C = C_i / M_i = C_j / M_j \quad . \quad [29]$$

1) Accuracy and Error Determination

a. Systematic Error Estimation

The perspective error which arises from unequal magnification of the fore and rear sections of an object, can be estimated by the correction terms (45)

$$h_i = x_{i,tr} - X_{i,j} = - \frac{(x_i + x_j) X_{i,j} \tan \sigma_1}{2 L_2} - \frac{(x_i + x_j) Y_{i,j}}{2 L_2} , \quad [30]$$

$$k_i = y_{i,tr} - Y_{i,j} = \frac{(x_i + x_j) X_{i,j}}{2 L_2} + \frac{(x_i - x_j) Y_{i,j} \cot \sigma_1}{2 L_2} , \quad [31]$$

$$\ell_i = z_{i,tr} / M_i - Z_{i,j} = - \frac{x_i (X_{i,j} \sin \sigma_1 - Y_{i,j} \cos \sigma_1)}{L_2} \quad [32]$$

and

$$\ell_j = z_{j,tr} / M_j - Z_{i,j} = \frac{x_j (X_{i,j} \sin \sigma_1 - Y_{i,j} \cos \sigma_1)}{L_2} \quad [33]$$

The tilt error that stems from a change in magnification which is caused when the axis of rotation does not coincide with the optical one, can be calculated by (45)

$$(M_i / M_j) = \frac{x_i - (x_j x_i / L_2) \operatorname{cosec} 2\sigma_1 + (x_i x_j / L_2) \cot 2\sigma_1}{x_j - (x_j x_i / L_2) \cot 2\sigma_1 + (x_i x_j / L_2) \operatorname{cosec} 2\sigma_1} \quad . \quad [34]$$

Under the operating conditions of our scanning electron microscope

$$L_2 = w M \qquad [35]$$

and so, for the employed angles of sight and value of L_2, one can neglect the two above-mentioned errors.

b. Operational Errors

The magnification of the microscope during operation was constant up to 1 - 1.5 % while the specification of the angle of sight was accurate by $1/2^{o}$.

2. Results

As the algebraic sign of x_i or x_j could not be ascertained, we calculated for each particle the possible values $L'_{i,j}$, $L''_{i,j}$ related to various pairs of angles, and decided upon the correct length by finding the matching pair (20) Results of typical determinations are shown in Table 6.

3. Discussion

The photogrammetric method seems to be operative; however, in passing from the simple shapes checked here to more complicated ones we may expect new difficulties Thus, the general problem of viewing the concave portions of a surface as well as its underneath sections can then arise (Fig. 15). Also, the actual number of points whose coordinates have to be analyzed, and the advantageous way of interpolation, should then be tackled.

In our method, the time necessary to observe one particle from three directions of sight is about 10 minutes, which is prohibitive for field purposes; however, there always exists the possibility of interfacing directly the signal data to a suitable computer.

Ordinal Number of particle	$L_{1,2}$ (μm)	$L_{2,3}$ (μm)	$L_{1,3}$ (μm)	L (μm)	C (μm)
1	33.9	35.9	21.1	14.8	1.0
	14.7	14.8	14.9		
2	69.5	71.4	15.1	14.6	1.0
	14.0	14.6	37.5		
3	21.9	12.3		12.3	0.90
	12.3	9.9			

Table 6: Typical Analysis of Results Acquired by Sighting the Particle at an Angle of : $1 - 0^{o}$, $2 - 20^{o}$, $3 - 40^{o}$ to the Normal of the Collecting Surface.

L — matched value of length

VI. DETERMINATION OF NUMBER CONCENTRATION

No attention has been paid in the first period of study to methods of determination of number concentration. The Derjagin-Vlasenko (28) or the filtration-counting (23, 24) techniques appear to be appropriate and easy to carry out. Consequently, we postponed this phase of study for more immediate and pressing needs.

VII. ASSESSMENT OF ELECTRIC CHARGE

The determination of the electric charge of a single aerosol particle and, hence, the charge-size distribution was chosen to be performed by measuring the velocity of motion in a combined gravitational and uniform electric field. As pointed our beforehand, the application of the method to even the simple case of a spin-free ($\vec{\omega} = \vec{0}$), symmetric particle ($\vec{\vec{C}} = \vec{\vec{0}}$) does require a knowledge of the translation tensor $\vec{\vec{K}}$. If one writes Eq. [7] in an explicit form based on a system of cartesian coordinates along the principal axes of translation x', y', z' and an external system x, y, z (6), then

$$\vec{v}_\infty = (1/\mu)\,\vec{\vec{K}}^{-1} \cdot (m\vec{g} + q\vec{E}) = (1/\mu)\,(\vec{i}'\vec{i}'\,K_1^{-1} + \vec{j}'\vec{j}'\,K_2^{-1}$$

$$+ \vec{k}'\vec{k}'\,K_3^{-1}) \cdot (mg\vec{k} + qE\vec{i}) \qquad [36]$$

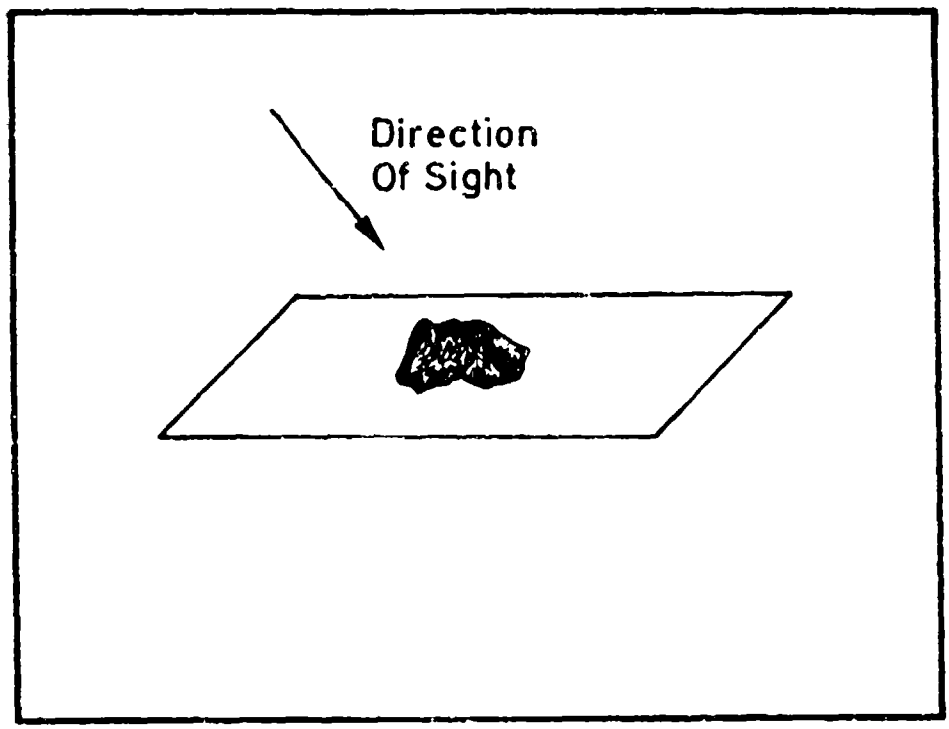

Fig. 15. Schematical Description of a "Problematic" Particle.

VI. DETERMINATION OF NUMBER CONCENTRATION

No attention has been paid in the first period of study to methods of determination of number concentration. The Derjagin-Vlasenko (28) or the filtration-counting (23, 24) techniques appear to be appropriate and easy to carry out. Consequently, we postponed this phase of study for more immediate and pressing needs.

VII. ASSESSMENT OF ELECTRIC CHARGE

The determination of the electric charge of a single aerosol particle and, hence, the charge-size distribution was chosen to be performed by measuring the velocity of motion in a combined gravitational and uniform electric field. As pointed our beforehand, the application of the method to even the simple case of a spin-free ($\vec{\omega} = \vec{0}$), symmetric particle ($\vec{\vec{C}} = \vec{\vec{0}}$) does require a knowledge of the translation tensor $\vec{\vec{K}}$. If one writes Eq. [7] in an explicit form based on a system of cartesian coordinates along the principal axes of translation x', y', z' and an external system x, y, z (6), then

$$\vec{v}_\infty = (1/\mu)\,\vec{\vec{K}}^{-1} \cdot (m\vec{g} + q\vec{E}) = (1/\mu)\,(\vec{i}'\vec{i}'\,K_1^{-1} + \vec{j}'\vec{j}'\,K_2^{-1}$$

$$+ \vec{k}'\vec{k}'\,K_3^{-1}) \cdot (mg\,\vec{k} + qE\,\vec{i}) \qquad [36]$$

or

$$(v_\omega)_x = \vec{i} \cdot \vec{v}_\omega = (1/\mu)[\ell_{11}(\ell_{31} mg + \ell_{11} qE) K_1^{-1}$$

$$+ \ell_{12}(\ell_{32} mg + \ell_{12} qE) K_2^{-1} + \ell_{13}(\ell_{33} mg + \ell_{13} qE) K_3^{-1}], \quad [31]$$

$$(v_\omega)_y = \vec{j} \cdot \vec{v}_\omega = (1/\mu)[\ell_{21}(\ell_{31} mg + \ell_{11} qE) K_1^{-1}$$

$$+ \ell_{22}(\ell_{32} mg + \ell_{12} qE) K_2^{-1} + \ell_{23}(\ell_{33} mg + \ell_{13} qE) K_3^{-1}] \quad [33]$$

and

$$(v_\omega)_z = \vec{k} \cdot \vec{v}_\omega = (1/\mu)[\ell_{31}(\ell_{31} mg + \ell_{11} qE) K_1^{-1}$$

$$+ \ell_{32}(\ell_{32} mg + \ell_{12} qE) K_2^{-1} + \ell_{33}(\ell_{33} mg + \ell_{13} qE) K_3^{-1}] \quad [39]$$

where $\ell_{i,j'}$ is the cosine between the coordinates axes i and j', etc. In principle, it is possible to determine both the charge q and the mass m of a simple particle after the rate of motion $|\vec{v}_\omega|$ is measured at two orientations Φ_1, ϕ_1 and Φ_2, ϕ_2 (Fig. 16).

The theoretical calculation of the translation tensor has been successful with regard to a sphere (46-48), a spheroid (47, 48) and an infinite circular cylinder (50), at Reynolds numbers much smaller than unity and for a continuous medium ($K_n \ll 1$). The case pertaining to a molecular regime ($K_n \gg 1$) has been computed in relation to a sphere (51), an infinite cylinder,

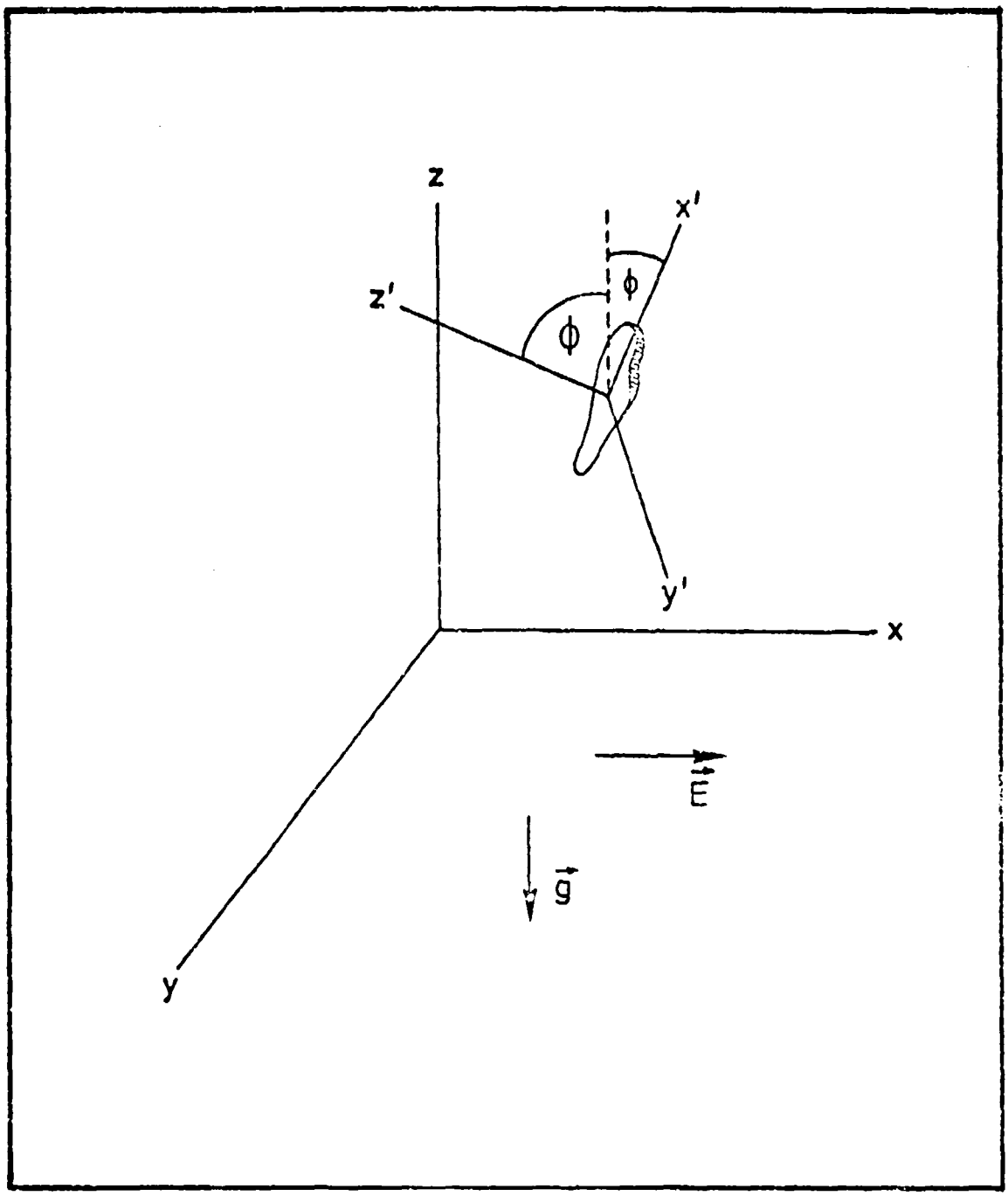

Fig. 16. Schematical Description of a Nonspherical Particle in a Gravitational-Electric Field.

a spheroid, and a cube (52). The extremely important situations concerning slip and transition flow have not been subjected to rigorous treatment and only an approximation procedure exists (53).

a. Resistance of an Ellipsoid to Creeping Motion at Very Small Knudsen Numbers

The translation tensor of an ellipsoid at creeping flow conditions and in a continuous medium has been calculated by Oberbeck to be (54)

$$\vec{\vec{K}} = 16\pi a b c \left[\langle \vec{i}\,\vec{i}/(\chi_0 + a^2\alpha_0) \rangle + \langle \vec{j}\,\vec{j}/(\chi_0 + b^2\beta_0) \rangle \right.$$

$$\left. + \langle \vec{k}\,\vec{k}/(\chi_0 + c^2\gamma_0) \rangle \right] \qquad [40]$$

where

$$\alpha_0 = abc \int_0^\infty d\lambda/(a^2+\lambda)\Delta\,, \quad \beta_0 = abc \int_0^\infty d\lambda/(b^2+\lambda)\Delta\,,$$

$$\gamma_0 = abc \int_0^\infty d\lambda/(c^2+\lambda)\Delta\,, \quad \chi_0 = \int_0^\infty d\lambda/\Delta\,, \text{ and } \Delta = [(a^2+\lambda)(b^2+\lambda)(c^2+\lambda)]^{1/2}.$$

These equations have been integrated only for the case of a spheroid as mentioned above (47); however, since a general ellipsoid suggests an extra degree of freedom in the simulation of a solid particle by that form, we thought it worthwhile to perform the integrations of [40] numerically. These were carried out according to Simpson's law using the Hebrew University CDC 6400 computer.

Results

The results of the integrations are brought out in Tables 7 through 9 and Figs. 17 through 19, where R_a, R_b and R_c, defined by

c/a / b/a	1	1.5	2	3	4	5	6	7	8	9	10
1	1		1.4086					3.0215	3.3095	3.5930	3.8686
1.5											
2			1.8673	2.2843	2.6805	3.0198	3.3823	3.6741	3.9946	4.3104	4.6162
3				2.7577	3.1254	3.5476		4.2474	4.5920	4.9319	5.2601
4					3.5993		4.4145	4.7753	5.1393	5.4989	5.8451
5						4.4833	4.8983	5.2732		6.0301	6.3915
6							5.3630		6.1444	6.5358	6.9103
7	3.0215							6.2004	6.6172	7.0220	7.4083
8									7.0759	7.4930	7.8899
9										7.9515	8.3581
10											8.8153

Table 7 : Resistance of an Ellipsoid to Motion in a Continuous Medium Along Axis a, R_a.

(a = 1 cm)

b/a \ c/a	1	1.5	2	3	4	5	6	7	8	9	10
1	1		1.266					2.1695	2.3912	2.5101	2.6746
1.5											
2			1.6287	1.8499	2.0617	2.2488	2.4519	2.6194	2.8029	2.9841	3.1605
3				2.2403	2.4254	2.6526		3.0336	3.2288	3.4194	3.6046
4					2.8092		3.2382	3.4335	3.6328	3.8311	4.0234
5						3.4003	3.6169	3.8163		4.2265	4.4249
6							3.9858		4.3989	4.6097	4.8134
7	3.0215							4.5518	4.7672	4.9834	5.1917
8									5.1280	5.3492	5.5618
9										5.7084	5.9250
10											6.2823

Table 8: Resistance of an Ellipsoid to Motion in a Continuous Medium Along Axis c, R_c.

(a = 1 cm)

c/a / b/a	1	1.5	2	3	4	5	6	7	8	9	10
1	1		1.4086					3.0215	3.3095	3.5930	3.8686
1.5											
2			1.6287	2.0068	2.3622	2.6772	3.0102	3.2865	3.5852	3.8797	4.1658
3				2.2403	2.5654	2.9277		3.5528	3.8607	4.1648	4.4601
4					2.8092		3.4978	3.8124	4.1287	4.4408	4.7441
5						3.4003	3.7446	4.0649		4.7079	5.0181
6							3.9858		4.6405	4.9672	5.2835
7	2.1695							4.5518	4.8869	5.2197	5.5417
8									5.1280	5.4666	5.7937
9										5.7684	6.0403
10											6.2823

Table 9: Resistance of an Ellipsoid to Motion in a Continuous Medium Along Axis c, R_c.

(a = 1 cm)

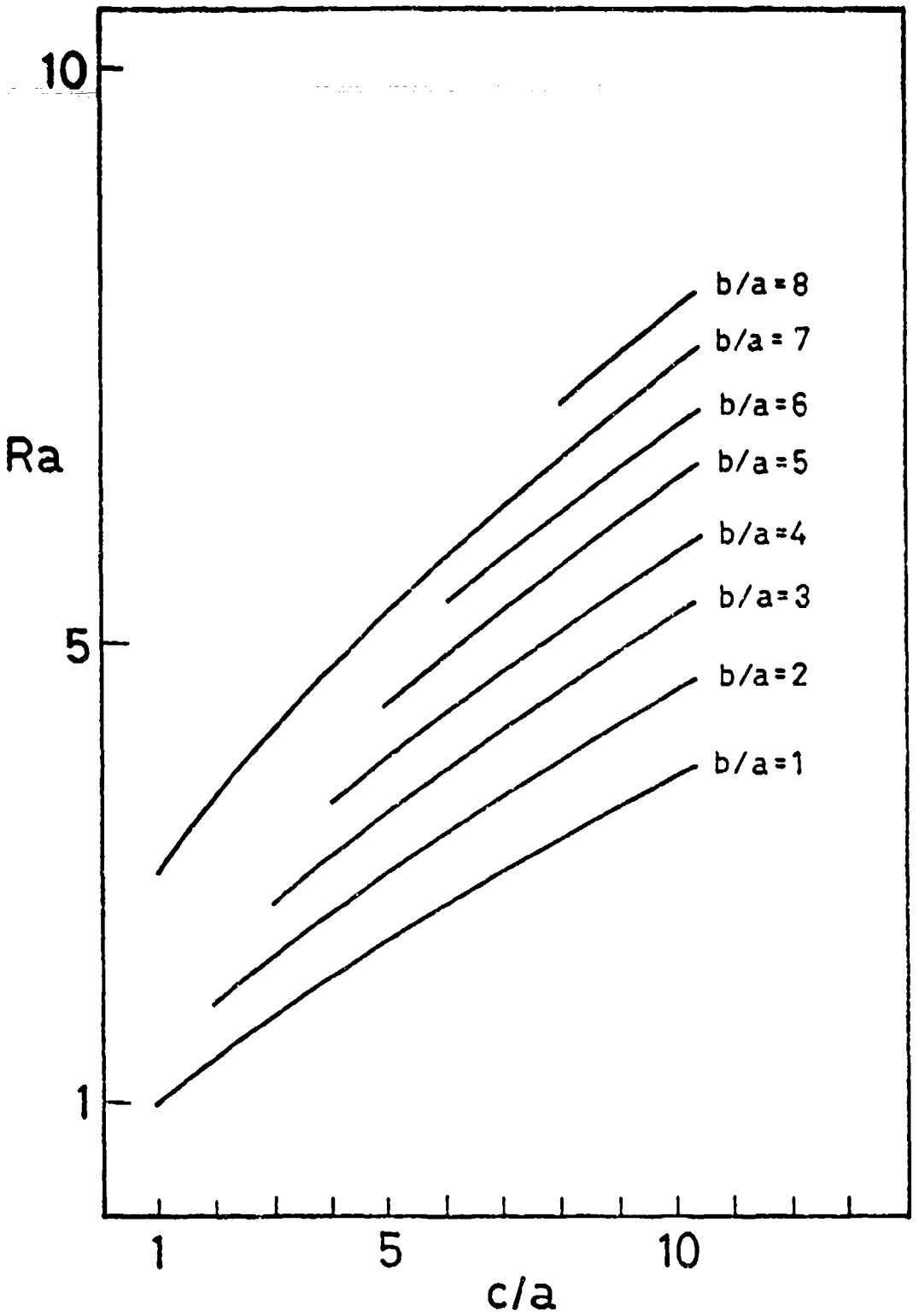

Fig. 17. Resistance of an Ellipsoid to Motion in a Continuous Fluid Along Axis α, R_α.
(a = 1 cm.)

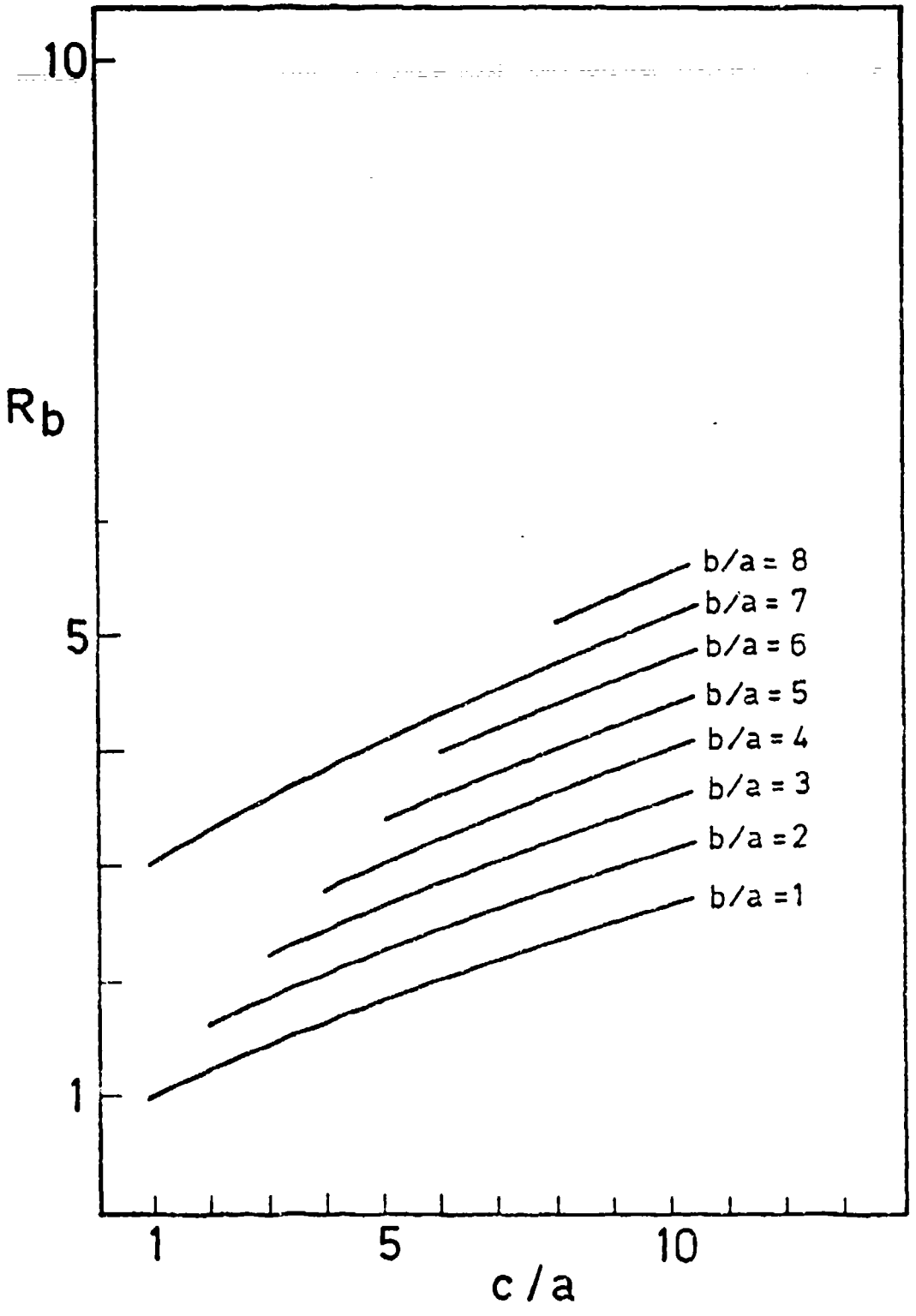

Fig. 18. Resistance of an Ellipsoid to Motion in a Continuous Fluid Along Axis ℓ, R_ℓ.

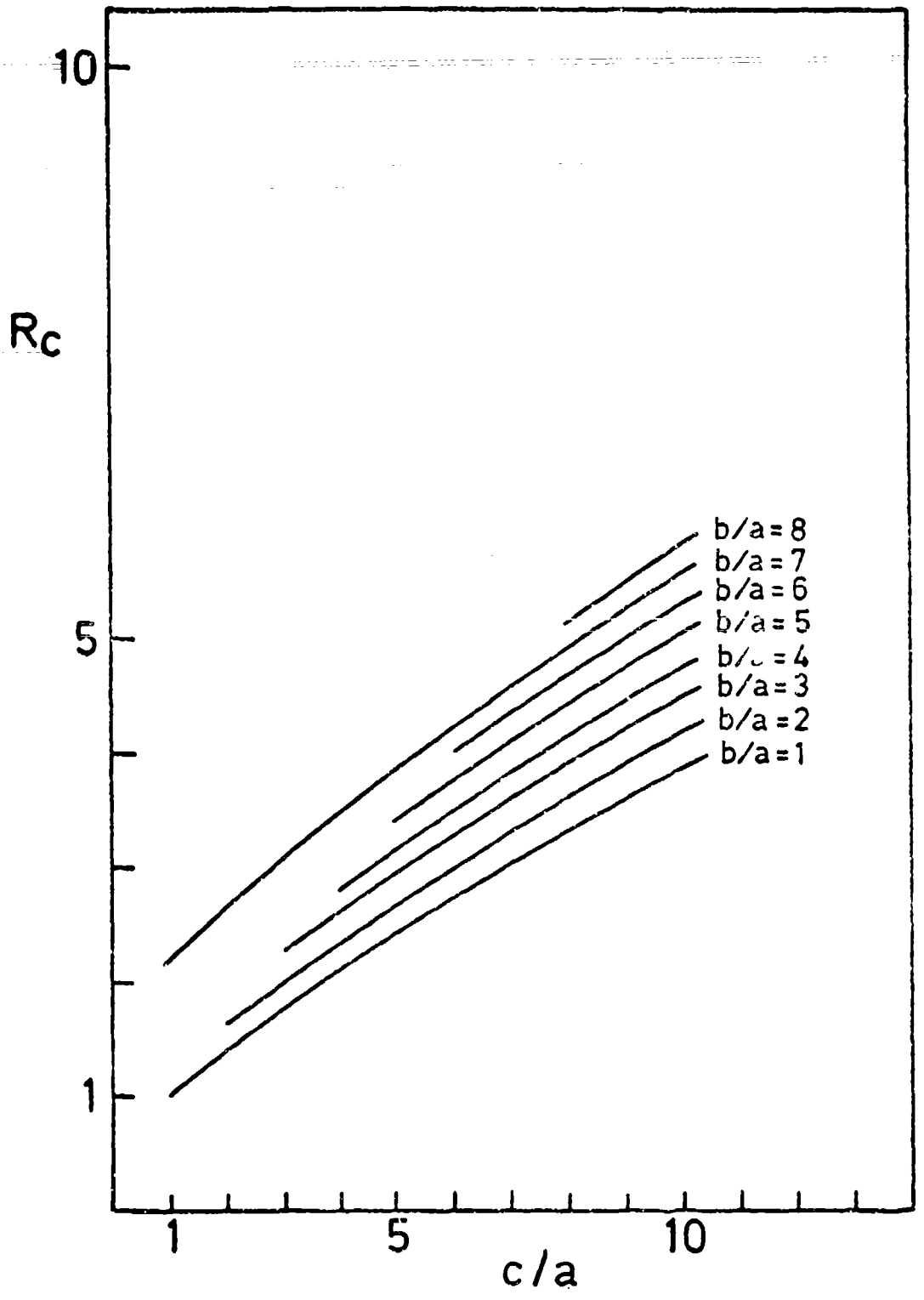

Fig. 19. Resistance of an Ellipsoid to Motion in a Continuous Fluid Along Axis c , R_c .

$$R_a = (8/3)\, abc/(x_o + a^2\alpha_o) \qquad [41a]$$

$$R_b = (8/3)\, abc/(x_o + b^2\beta_o) \qquad [41b]$$

$$R_c = (8/3)\, abc/(x_o + c^2\gamma_o) \qquad [41c]$$

are the radii of a sphere having the same resistance to motion as an ellispoid that translates along axis a, b or c, respectively. The accuracy of the calculations was determined by a comparison between the values for rotational ellispoids and those obtained by the analytical procedure (55).

Discussion

It turns out that the accuracy depends on both the interval step and the value for the upper limit of the integrals; however, whereas the convergence of the solutions as a function of $\Delta\lambda$ is very fast, most of the problem is due to the finiteness of the limit. The smaller the product abc the lower is the value of the upper limit which is necessary to achieve a specific accuracy, or in other words, the greater the ratios b/a and c/a, the higher should be the said limit.

The accuracy of the integrations is of the order of 3%, which is sufficient for our purposes. It can be increased but only at a considerable expense of computer time.

From the results, one can see that the influence of the asymmetry of the ellipsoid may reach the order of a couple of hundred percent.

b. Effect of Brownian Rotation

The motion of a nonspherical particle may be complicated due to an interaction between translation and rotation which constantly changes the orientation

angles. The interaction can be caused both by a fluid dynamic effect ($\vec{C} \neq \vec{0}$) and by the unbalanced impacts of the molecules of the medium which bring forth a rotational Brownian movement. For some symmetrical forms the first factor vanishes ($\vec{C} = \vec{0}$) whereby the orientation of the particle becomes neutrally stable. On the other hand, the Brownian action does always remain.

The extent of Brownian rotation in a continuous fluid is given for a sphere by (56)

$$\overline{\theta_1^2} = 2\, D_{r,s}\, t = (2kT/8\pi\mu r^3)\, t \qquad [42]$$

and for a spheroid of $b_1 \gg a_1$ which turns about its equatorial axis, by (56) *

$$\overline{\theta_1^2} = 2 D_{ell.}\, t = 2\,[kT/\langle 8\pi\mu b_1^3/3(\ln(2b_1/a_1) - 0.5)\rangle]\, t. \qquad [43]$$

The times necessary to achieve a root mean square angle of 45° are shown in Tables 10 and 11.

From these tables it is immediately perceived how <u>inherently stochastic</u> is the orientation of a nonspherical aerosol particle as well as its whole motion (Equs. [37] through [39]). In essence, the movement of such a particle may be considered as a series of random flights of a variable step length. Thus,

---

* The restriction to $b_1 \gg a_1$ is not needed since one may use for the mobility of a prolate ellipsoid the expression (57) :

$$B = 3\left\{\frac{2(b_1/a_1)^2 - 1}{\langle (b_1/a_1)^2 - 1\rangle^{1/2}} \ln\left[(b_1/a_1) + \langle (b_1/a_1)^2 - 1\rangle^{1/2}\right] - (b_1/a_1)\right\} \Big/ 16\pi\mu a_1^3 \langle (b_1/a_1)^4 - 1\rangle \,. \qquad [44]$$

d (μm)	time in air at 1 atm. (sec.)	time in water (sec.)
0.4	0.00028	0.015
1	0.0044	0.24
2	0.035	1.9
4	0.28	15
10	4.4	240
20	35	1900
40	280	15000
100	4400	240 000
200	35000	1 900 000

Table 10 : Rotational Brownian Movement of Spheres.
Times (sec.) Needed for a Root Mean Square
Rotation of 45° at 20° C (56)

C (μm) / L (μm)	0.2	0.5	1	2	5	10
	Air at 1 atm.					
1	0.00081					
2	0.0047	0.0075				
5	0.054	0.074	0.102			
10	0.36	0.44	0.59	0.81		
20	2.5	3.0	3.7	4.7	7.4	
100	229	267	306	358	435	810
200	1650	1910	2130	2450	3020	3680
	water					
1	0.045					
2	0.26	0.41				
5	3.0	4.1	5.7			
10	20	24	33	45		
20	136	168	204	260	410	
100	12700	14800	17000	19900	24200	45000

Table 11: Rotational Brownian Movement of Rod Shaped (Ellipsoidal Needle-like) Particles. Times (sec.) Needed for a Root Mean Square Rotation of 45^{o} at $20\,^{o}C$ (56).

on the conditions of a fast relaxation time τ (55), one would have

$$(\vec{v}_j)_{t_j \to t_j + \Delta t_j} \cong (\vec{v}_j)_{\infty, t_j} \qquad [45]$$

and

$$\vec{s}_j \cong \int_{t_j}^{t_j + \Delta t_j} (\vec{v}_\xi)_\infty \, d\xi \qquad [46]$$

where

$$(\vec{v}_j)_{\infty, t_j} = (\vec{v}_j)_{\infty, t_j} \left(\phi_{t_j}, \psi_{t_j}, K_1, K_2, K_3, \sum_i \vec{F}_{ix,i} \right), \qquad [47]$$

the orientation angles themselves determined by a probability function

$$P \left(\phi_{t_j} - \phi_{t_j - \Delta t_j}, \phi_{t_j} - \phi_{t_j - \Delta t_j}, K_1, K_2, K_3 \right). \qquad [48]$$

The averaging of the stochastic motion is still carried out by the procedure (58, 59)

$$\overline{\vec{v}_\infty} = \vec{F}_{ex} \left[1 / \overline{K_j (\phi_{j,\vec{s}}, \psi_{j,\vec{s}})} \right]_{j = 1,2,3} ; \qquad [44]$$

however, a new way of calculation has been lately suggested in a computational (55) and theoretical (60) study where the velocity of the particle is expressed by

$$\vec{v}_\infty = \vec{F}_{ex} \left\{ \overline{1 / K_j (\phi_{j,\vec{s}}, \psi_{j,\vec{s}})} \right\}_{j = 1,2,3} . \qquad [50]$$

On the experimental side of the problem, there has not been any quantitative investigations related to the Brownian rotation of an aerosol particle. Thus, as the phenomenon is of great practical importance, we set out to perform a preliminary series of experiments.

(1) Experimental

Schematically, a typical trajectory of a sedimenting particle in a neutrally stable orientation may look as shown in Fig. 20. So, one can expect that, because of Brownian rotation, the overall drift of such a particle should diminish with time. The extent of this effect constituted the aim of our experiments.

In these experiments a model aerosol of glass fiber particles (Chap. IV b) was introduced into a sedimentation chamber A having for a bottom a diaphragm with a centrally located, wedge-shaped hole (Fig. 21). Below the diaphragm there was placed a scanning electron microscope stub B to whose surface a cover glass had been cemented as mentioned above. The distance between the stub and the hole C could be varied, thus affecting the time available for a particle to change its orientation. The actual procedure consisted of sucking into the chamber a test aerosol which settled down under convection-free conditions. After an elapse of sufficient time, the stub B was dissembled, gold shadowed (Chap. V), and then observed in the scanning electron microscope.

To measure the "smearing out" influence of the Brownian movement, we determined the maximal angle of overall drift Ψ (Fig. 20) by locating the particle situated farthest from the center of the stub. This particle was photographed from three directions of sight and its dimensions calculated according to our photogrammetric method. Actually, since each measured particle could have fallen through the diaphragm hole at points bounded by the two extremes A and B (Fig. 20), the indeterminacy in Ψ amounted to

$$\Delta\Psi = \tan^{-1}(d_A/h_o) - \tan^{-1}(d_B/h_o) \quad . \qquad [51]$$

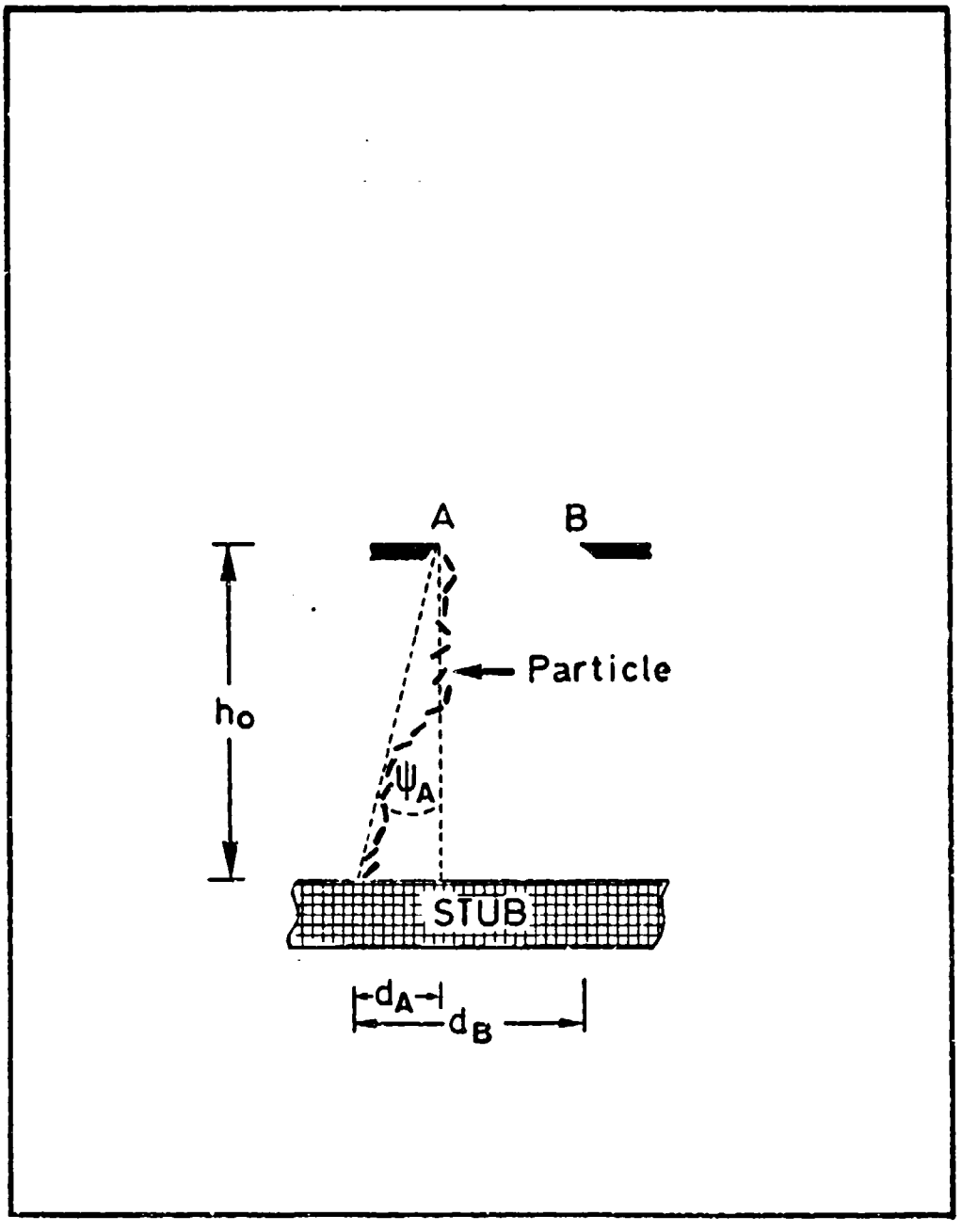

Fig. 20 Typical (Projected) Trajectory of a Sedimenting, Rotating Particle.

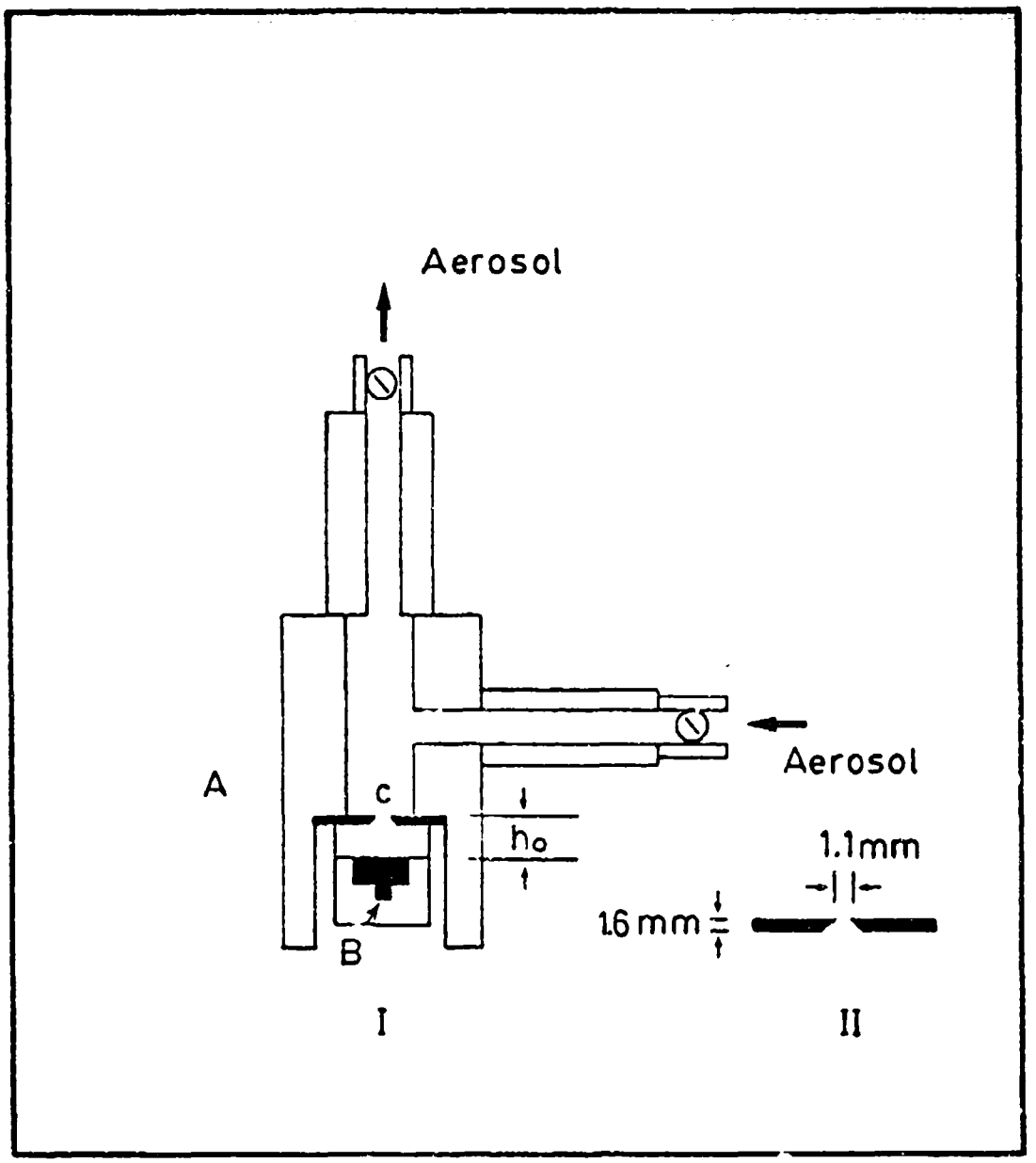

Fig. 21. Sodimentation Cell for the Determination of "Orientation-Averaging" (Schematical).
I - Cell, II - Diaphragm.

As a precaution, we checked the possible influence of electric charges on the trajectory of the particles by comparing results first while using a dielectric diaphragm and secondly employing a brass one. The pattern of the sediment in the two cases was observed under a light microscope and the difference seen to be negligible. The center of the stub was found by a simple geometric way during observation in the scanning electron microscope. Also, the position of the diaphragm hole relatvie to the center was ascertained by the aid of a bulky deposit of talc particles which were allowed to fall in the sedimentation chamber.

Results

The angles of overall drift were determined for various depths and compared with the maximal deflections calculated from continuous fluid dynamics according to (fig. 22) (61)

$$(\tan\Psi)_t = (u_x)_\infty / (u_z)_\infty = -\sin 2\Phi / \left[\frac{1/2 - 3\ln(L/C)}{3/2 - \ln(L/C)} + \cos 2\Phi \right] \qquad [52]$$

which gives

$$(\tan\Psi)_{t,m} = -\frac{(A_3^2 - 1)^{1/2}}{A_3^2 - 1} \qquad [53]$$

where

$$A_3 = \frac{1/2 - 3\ln(L/C)}{3/2 - \ln(L/C)} \quad .$$

The results are presented in Table 12, in Figs. 23 through 27, and in the summarizing Fig. 28.

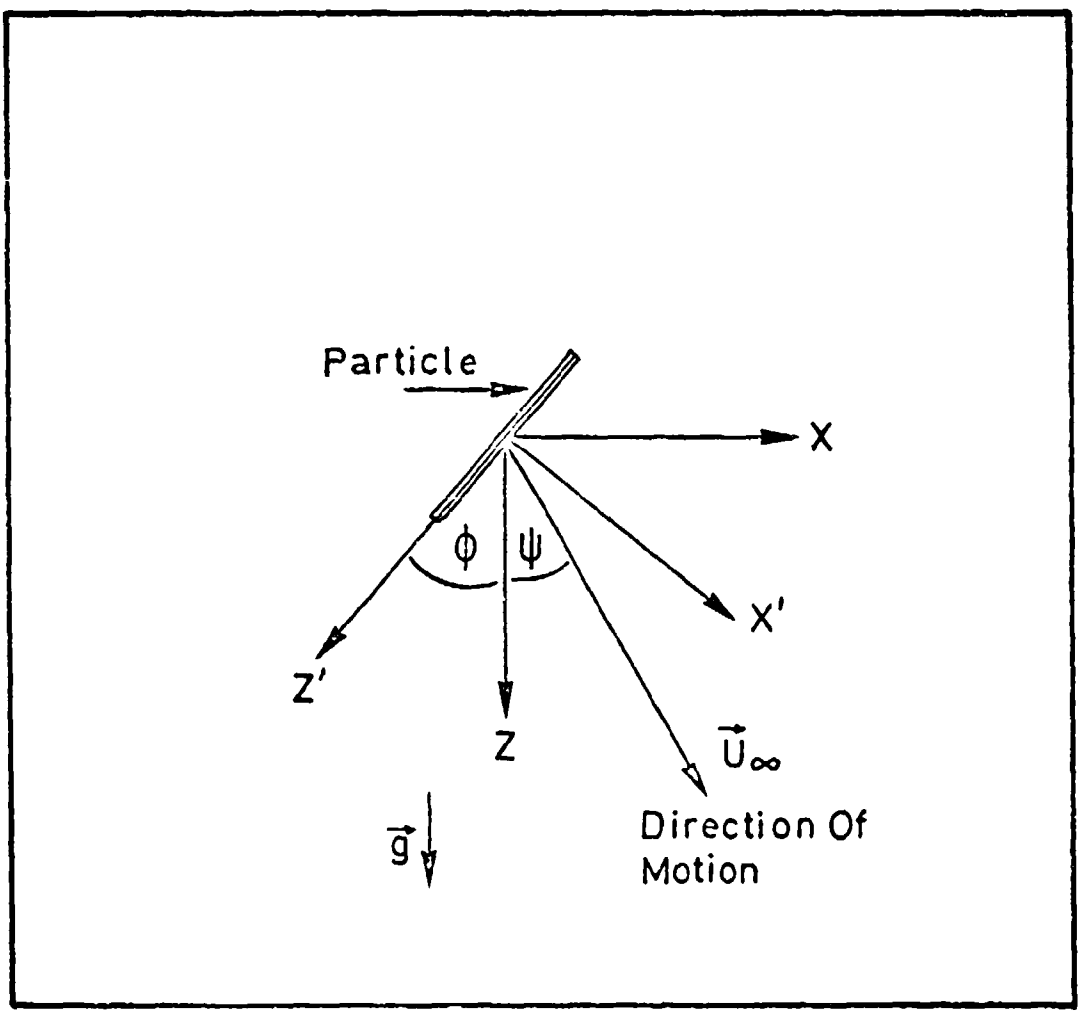

Fig. 22. Oblique Fall of a Cylindrical Particle.

L(μm)	C(μm)	L/C	$(\tan \Psi)_A$	$(\tan \Psi)_B$	$(\tan \Psi)_{tm}$
h_0 = 2.65 mm					
10.2	0.23	44.6	0.04	0.46	0.22
38.6	0.47	81.4	0.06	0.47	0.23
32.8	0 55	59.7	0.01	0.43	0.22
50.3	0.30	167.6	0.07	0.49	0.25
27.0	1.18	22.9	0.00	0.41	0.19
h_0 = 3.15 mm					
14.8	0 96	15.4	1.36	1.71	0.21
14.6	1.0	14.6	0.13	0.48	0.16
12.3	0.88	14.0	0.35	0.70	0.15
h_0 = 4.20 mm					
7.6	0.34	22.2	0.10	0.36	0.18
6.6	0.47	14.0	0.00	0.26	0.15
6.9	0.14	47.5	0.13	0.39	0.22
20.8	1.23	16.9	0.00	0.26	0.17
25.6	1.68	15.2	0.13	0.40	0.16

Table 12: Overall Drift Angles of Cylindrical Particles for Various Depths of Fall.

Table 12 : (cont'd)

L (μm)	C (μm)	L/C	$(\tan \Psi)_A$	$(\tan \Psi)_B$	$(\tan \Psi)_{t,m}$
h_0 = 5.20 mm.					
6.1	0.36	17.0	0.72	0.93	0.17
11.8	0.21	56.9	0.14	0.35	0.22
h_0 = 5.85 mm.					
2.70	0.24	11.3	0.21	0.40	0.14
3.8	0.18	20.7	0.05	0.24	0.18
21.4	0.70	30.3	0.08	0.27	0.20
21.9	0.46	54.8	0.03	0.21	0.22
18.2	0.22	83.8	0.08	0.26	0.23
33.5	0.45	73.5	0.03	0.22	0.23
h_0= 7.55 mm.					
9.9	1.43	6.94	0.10	0.24	0.07
29.8	2.75	10.8	0.32	0.47	0.13
10.6	0.25	42.6	0.70	0.84	0.21
8.2	1.1	7.42	0.49	0.64	0.09

Table 12: (Cont'd)

L (μm)	C (μm)	L/C	$(\tan\Psi)_A$	$(\tan\Psi)_B$	$(\tan\Psi)_{t.n}$
h_0 = 10.75 mm.					
3.6	0.26	13.7	0.41	0.52	0.16
8.5	0.27	31.5	0.42	0.52	0.20
h_0 = 10.9 mm					
7.5	0.88	8.85	0.02	0.12	0.11
8.5	0.50	17.1	0.00	0.10	0.17
13.8	0.47	10.3	0.00	0.10	0.14
19.6	1.13	17.7	0.03	0.13	0.17
h_0 = 10.95 mm.					
9.8	1.11	8.8	0.02	0.12	0.11
10.1	1.25	8.1	0.04	0.14	0.10

Table 12 : (cont'd)

L (μm)	C (μm)	L/C	$(\tan \Psi)_A$	$(\tan \Psi)_B$	$(\tan \Psi)_{A,m}$
h_0 = 14.85					
2.0	0.18	10.9	0.00	0.07	0.13
2.0	0.10	20.9	0.10	0.17	0.18
2.1	0.54	3.9	0.03	0.10	0.04
4.5	0.18	25.2	0.10	0.17	0.19
33.0	1.0	33.0	0.03	0.10	0.20
h_0 = 16.35 mm					
10.9	0.32	34.3	0.11	0.17	0.20
13.1	0.77	17.0	0.08	0.14	0.17
5.1	0.51	10.0	0.13	0.20	0.13
5.2	0.19	26.5	0.16	0.23	0.19
13.7	0.40	34.4	0.04	0.11	0.20
4.2	0.28	15.3	0.11	0.18	0.16
7.1	0.34	21.3	0.10	0.17	0.17
14.2	0.36	39.2	0.04	0.10	0.21

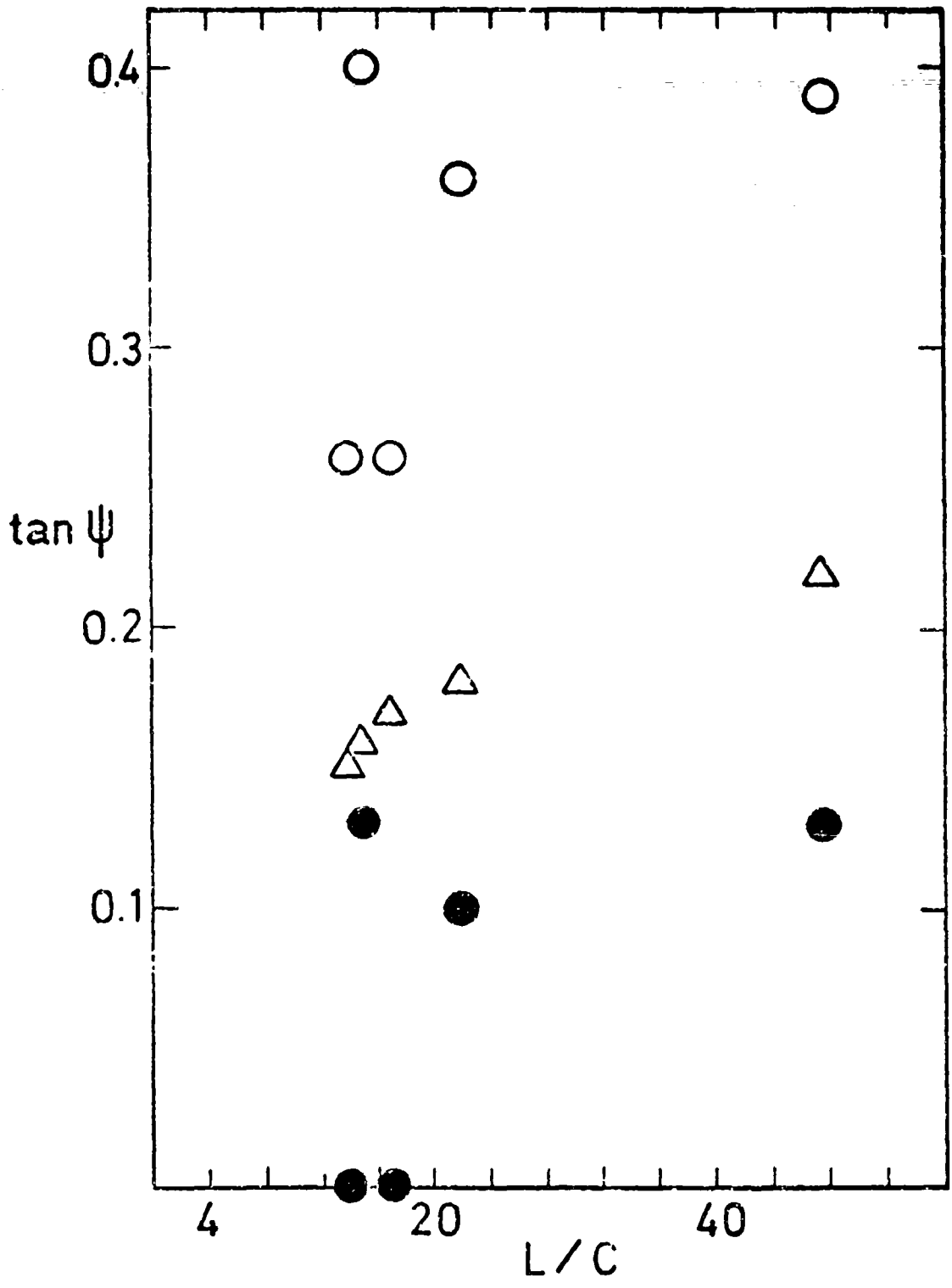

Fig. 23. Overall Drift Angle of Cylindrical Particles vs. Ratio of Length to Diameter.

h_0 = 4.20 mm., ● - $\tan \Psi_A$, o - $\tan \Psi_B$, Δ - $\tan \Psi_{s,m}$

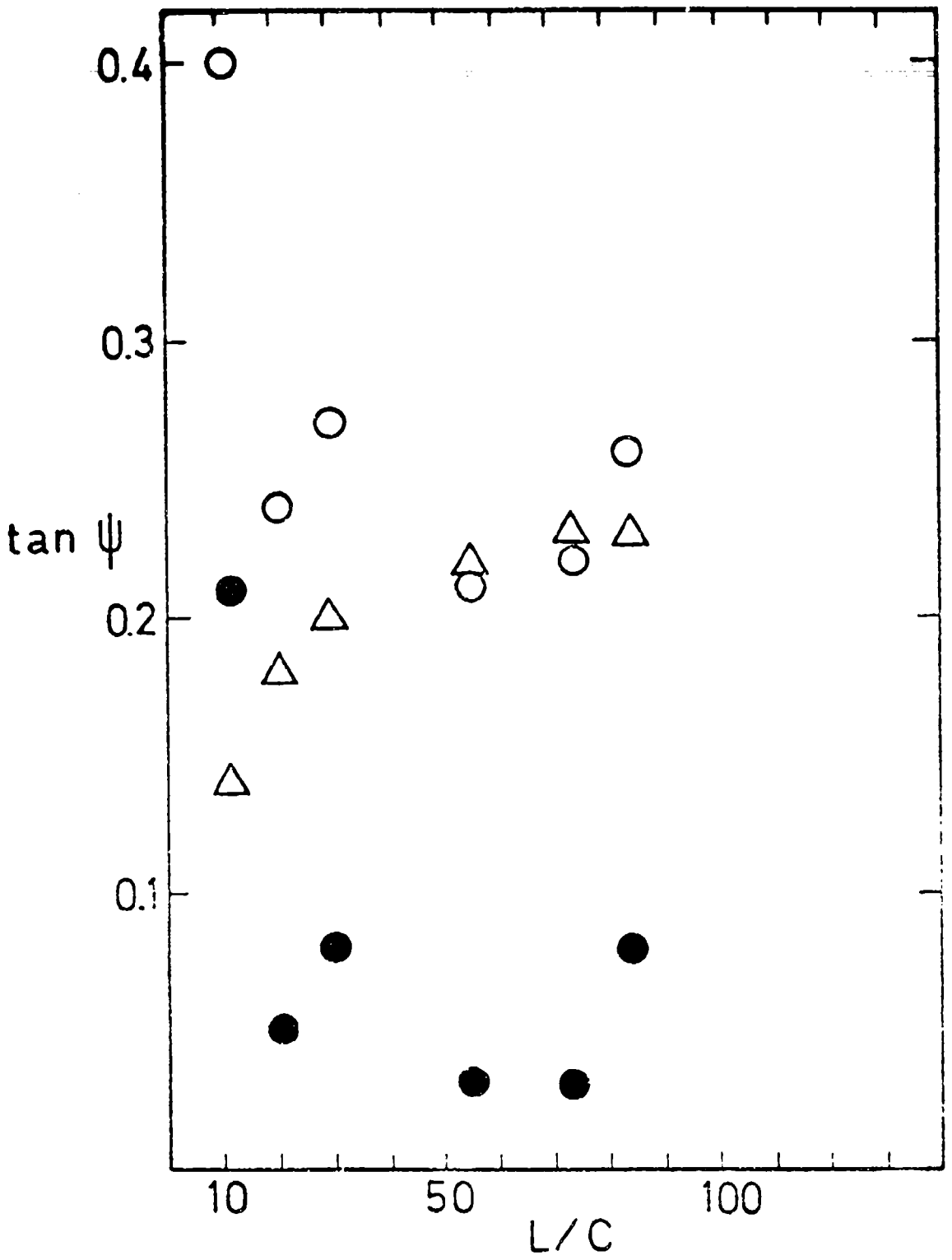

Fig. 24. Overall Drift Angle of Cylindrical Particles vs. Ratio of Length to Diameter.

h_0 = 5.65 mm., ● - $\tan \Psi_\alpha$, o - $\tan \Psi_\beta$, ▽ - $\tan \Psi_{\tau,m}$

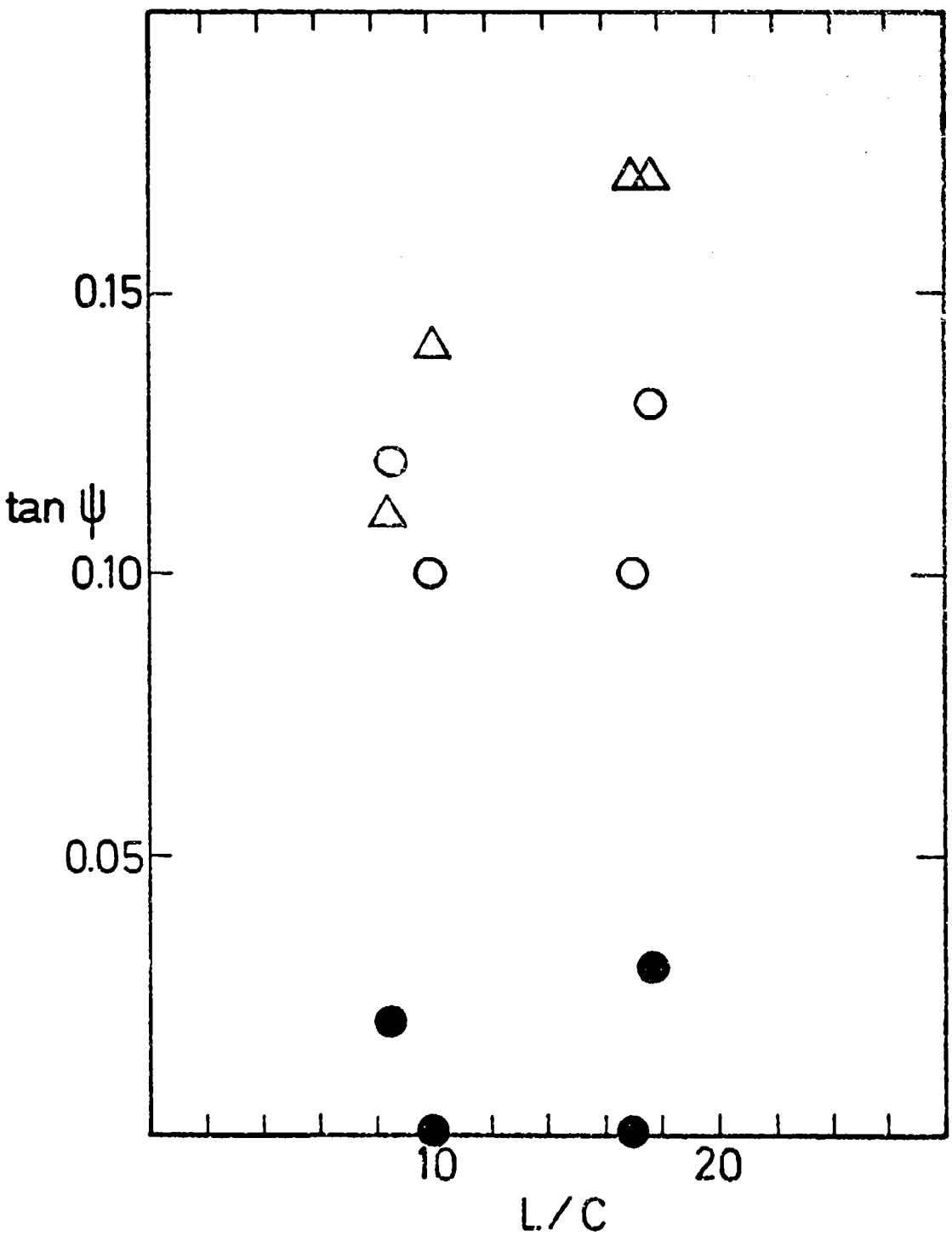

Fig. 25. Overall Drift Angle of Cylindrical Particles vs. Ratio of Length to Diameter.

h_0 = 10.9 mm., ● - $\tan \Psi_A$, o - $\tan \Psi_B$, ▽ - $\tan \Psi_{t,m}$

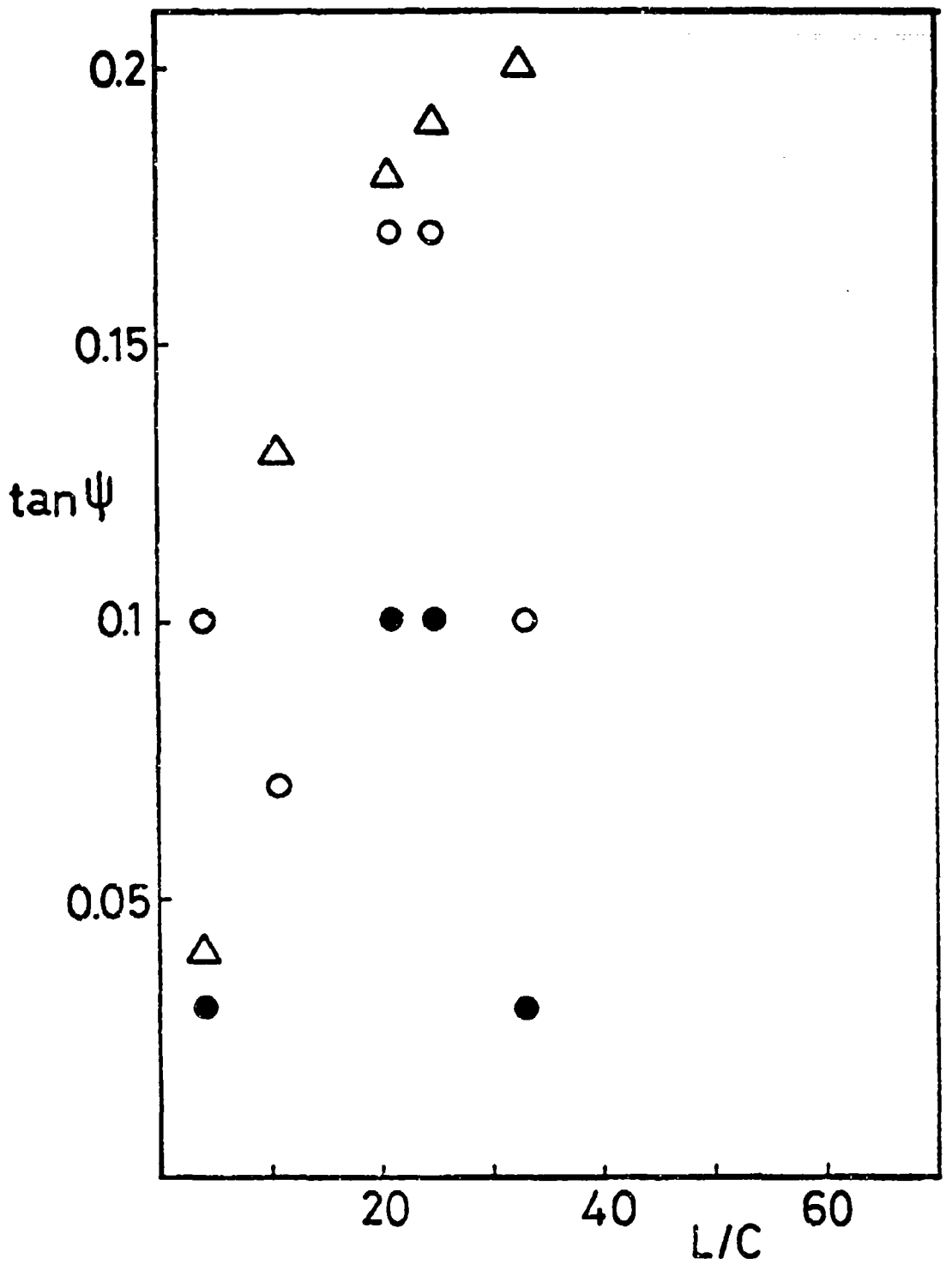

Fig. 26. Overall Drift Angle of Cylindrical Particles vs. Ratio of Length to Diameter.
h_0 = 14.85 mm., ● - $\tan\Psi_\beta$, ○ - $\tan\Psi_\beta$, ▽ - $\tan\Psi_{t,m}$

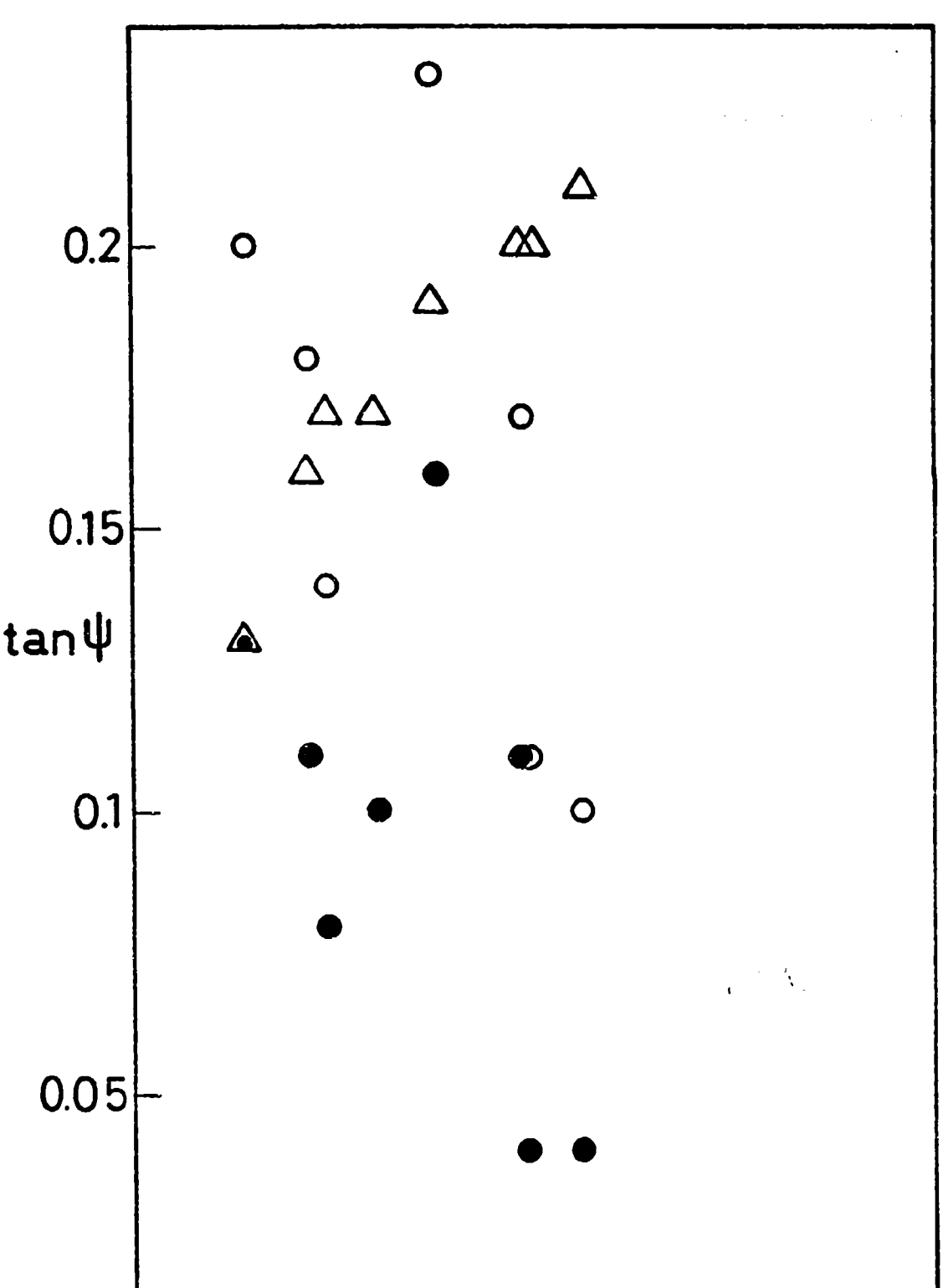

Fig. 27. Overall Drift Angle vs. Ratio of Length to Diameter.

h = 16.35 mm., ● - tan Ψ_a, ○ - tan Ψ_a, ∇ - tan $\Psi_{a,m}$

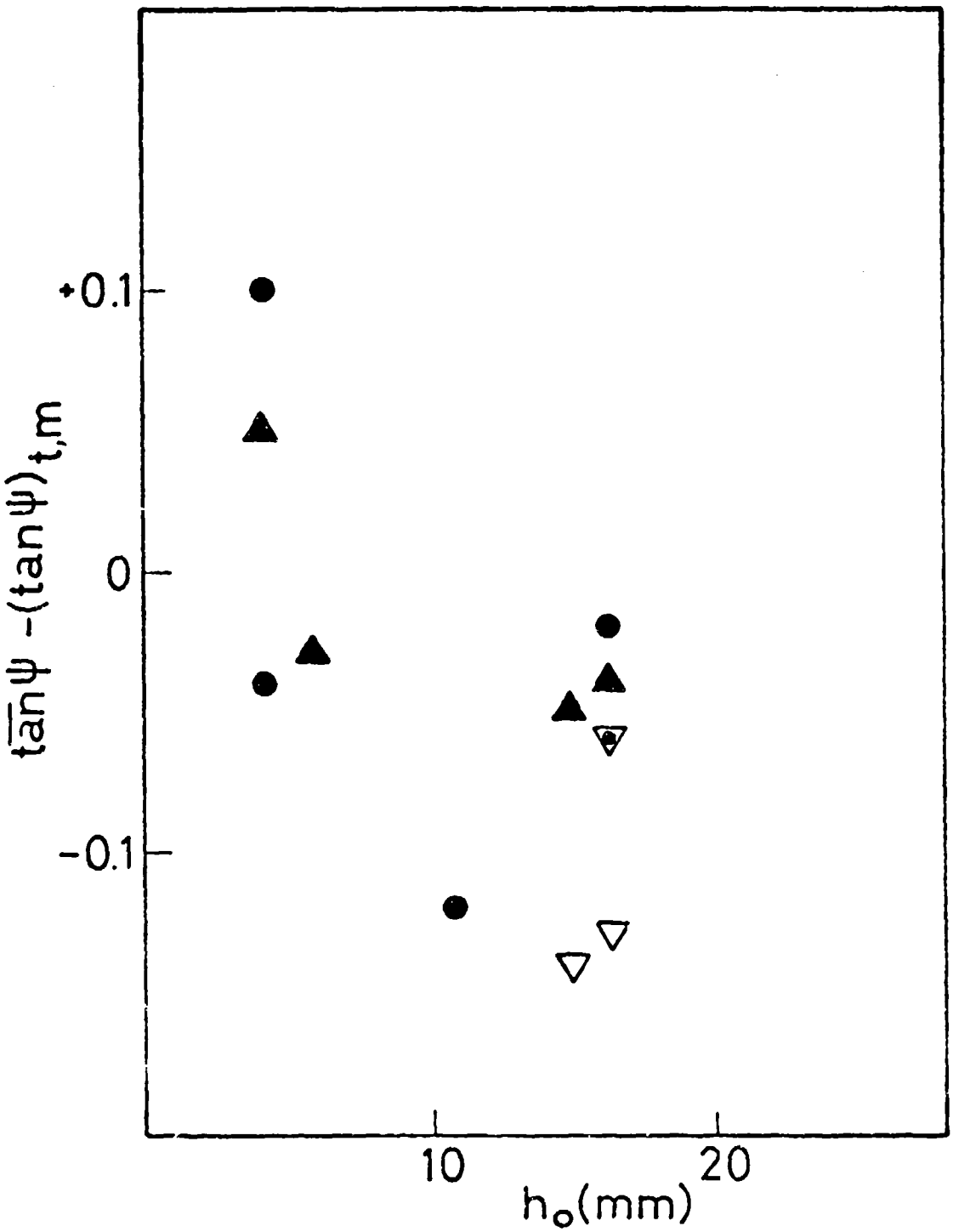

Fig. 28 ($\overline{\tan\psi} - \tan\psi_{t,m}$) vs. Depth of Fall of Cylindrical Particles for Various Ratios of Length to Diameter.

● - L/C = 15 - 17 ; ▲ - L/C = 20 - 22 ; ▽ - L/C = 30 - 35

Discussion

From these results one sees that:

1. The overall trajectory of our cylindrical partilces is not in the direction of gravity
2. The maximal, overall drift angle is indeed decreasing with time
3. The "smearing out" of the orientatior effect is not complete even in times of the order of 10 - 100 sec., so that the distribution of overall drift angles has to be taken into account
4. The maximal, overall drift angles are occasionally greater than those computed on continuous fluid assumptions.

The last finding may be ascribed to the "slip flow", in which resistance to motion is smaller than that calculated from classical fluid dynamics. If we express the principal resistances of a cylindrical particle by the intermediate regime equations

$$K_1^{*-1} = K_1^{-1} \left(1 + A_4 \bar{\ell}/L\right) \qquad [54]$$

and

$$K_3^{*-1} = K_3^{-1} \left(1 + A_5 \bar{\ell}/C\right) \qquad [55]$$

where K_1, K_3 are the continuous dynamics values and A_4, A_5 are surface-dependent constants of the order of unity (62), then (6)

$$\alpha \equiv (\tan\Psi)^*_{t,m} / (\tan\Psi)_{t,m}$$

$$= \frac{(K_1^{*-1} - K_3^{*-1})(K_1^{-1}\sin^2\phi + K_3^{-1}\cos^2\phi)}{(K_1^{-1} - K_3^{-1})(K_1^{*-1}\sin^2\phi + K_3^{*-1}\cos^2\phi)}, \qquad [56]$$

Some typical values of α are brought out in Table 13.

(ii) Motion of a Cylindrical Particle in a Liquid

At this stage we thought it worthwhile to check the continuous fluid equations by repeating the set of experiments of part (i) in a liquid medium. The results from these experiments would not be applicable to the transition regime but would represent the situation for $Kn \ll 1$. The sedimentation cell designed for this purpose consisted of (Fig. 29) a chamber A, a scanning electron microscope stub B, and a drainage arrangement C.

Experiments along this line are still in progress.

c. Determination of the Principal Resistances of Nonspherical Particles

From our analysis it seems that the logical way to study the movement of a nonspherical particle is the application of a random flight treatment to the constantly changing fluid dynamic resistance, and the employment of suitable equations of motion for each time interval.

The principal resistances of solid particles have been determined theoretically for a few cases of interest; no systematic, experimental investigation in this area has been carried out. Thus, we started a study towards the measurement of the resistances, which links with the second-year stage of the project.

Experimental

The apparatus constructed for this purpose (Fig. 30) consisted of a stereo-sedimentation chamber A where it was possible to observe a falling particle from two directions of sight ($\delta = 120^{o}$), and a vacuum system B (Fig. 31) with the aid of which the total pressure of the medium could be reduced. As the mean free path of the gas molecules is inversely proportional to the pressure, one may study the role of the Knudsen number $Kn (= \bar{\ell} / L$ while keeping the aerosol properties constant (63).

The trajectory of a falling particle was observed and recorded by low-magnification microscopes and suitable cameras G_1, G_2 (Fig. 31) (Olympus,

C/2 (μm)	L (μm)	L/(C/2)	ϕ (°)	α
0.05	2.5	50	30	2.46
			40	2.75
			54.8 *	3.42
0.1	5	50	30	2.04
			40	2.19
			54.8 *	2.55
0.2	5	25	30	1.77
			40	1.86
			54.8 *	1.90

Table 13: The Ratio α for Various Cylindrical Particles.

A_4, A_5 and $\bar{\ell}$ are taken to be 0.9, 0.9, and 0.1 um, respectively.

* — Orientation of maximal drift angle ($\Psi'_{e,m} = 19.5^{O}$) according to continuous fluid dynamics.

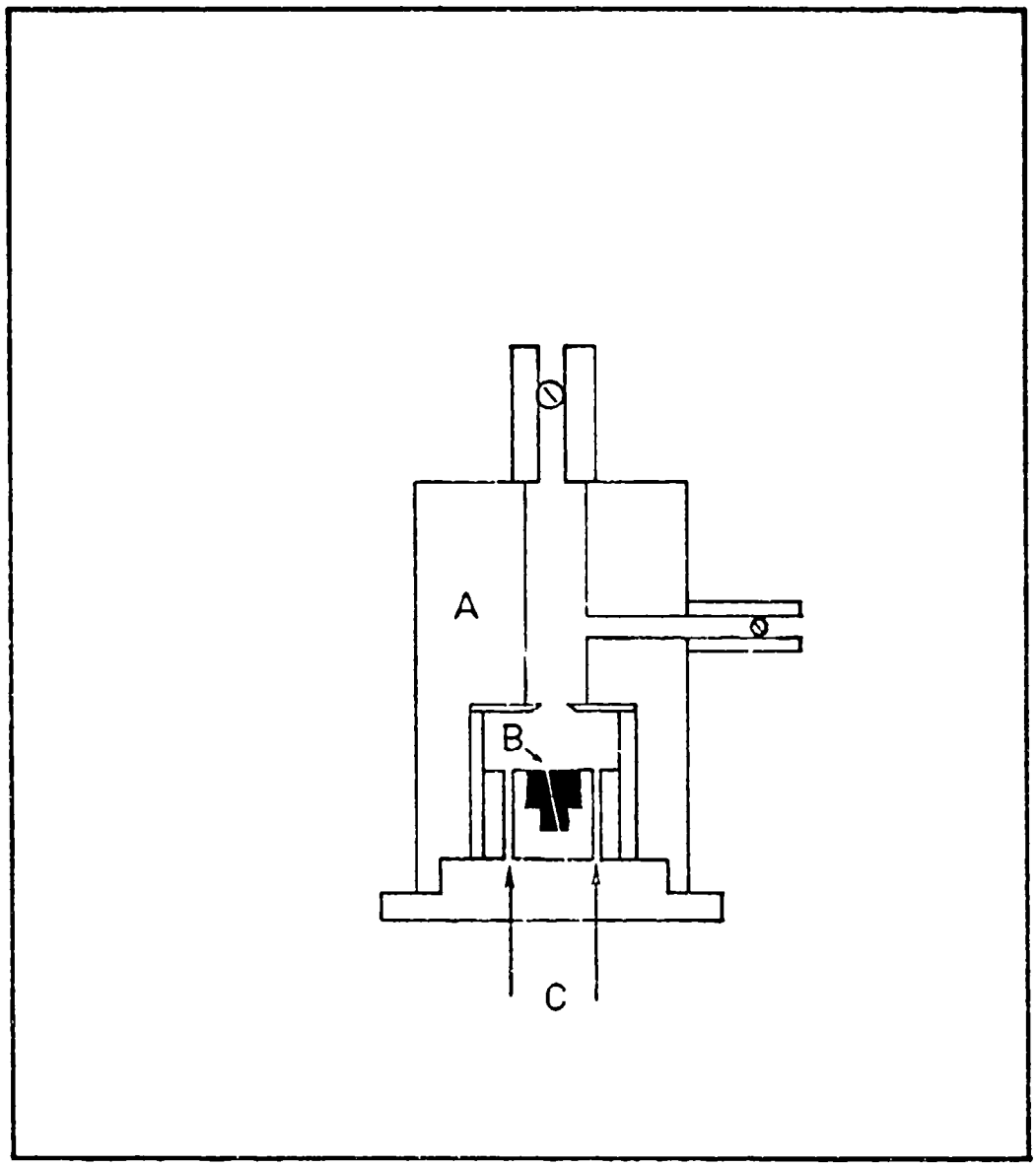

Fig. 29. Sedimentation Cell for Experiments on Brownian Rotation in Liquids (Schematical).

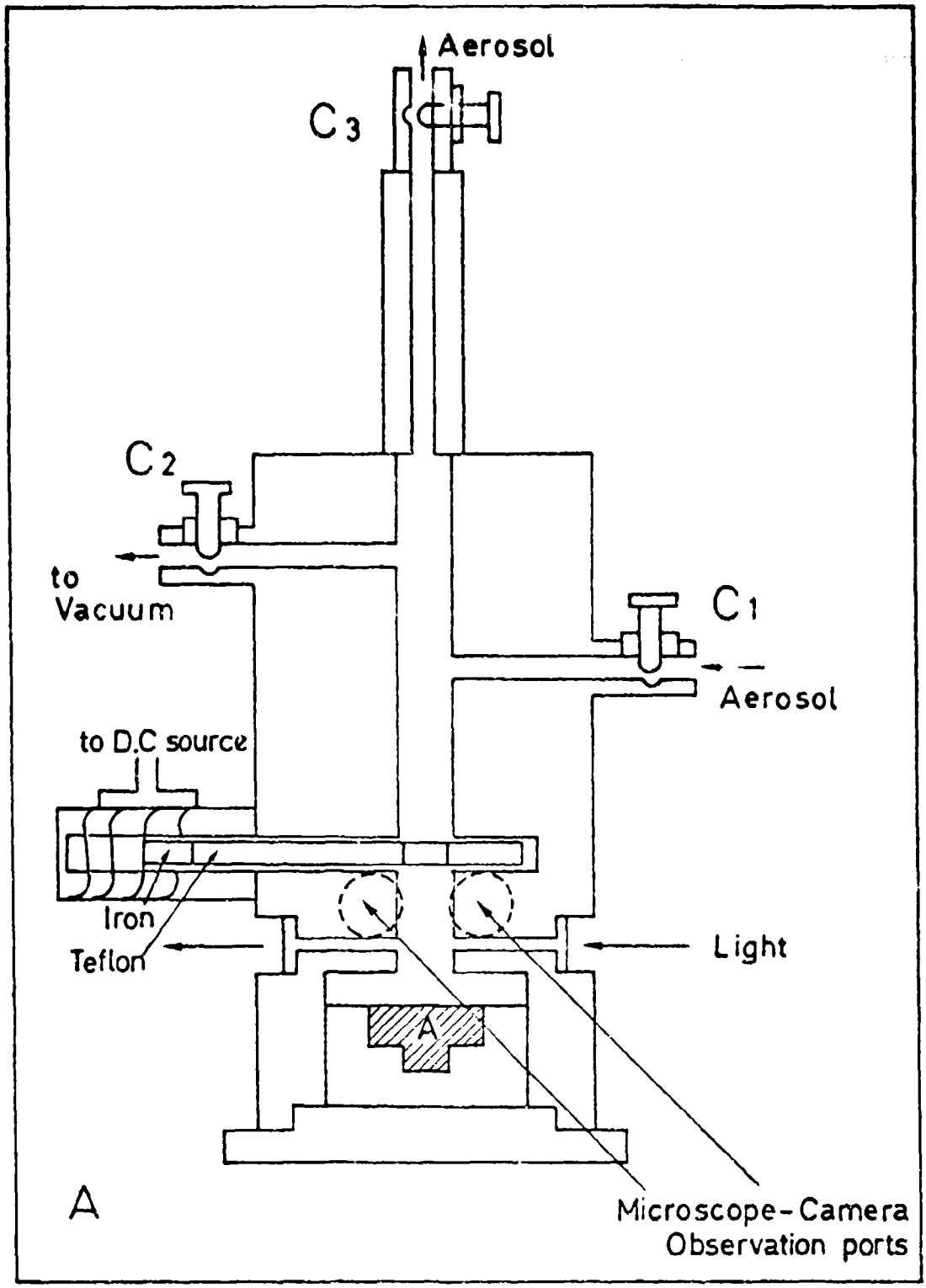

Fig. 30. The Stereo-sedimentation Cell (Schematical).

A - Stub of a Scanning Electron Microscope,

B - Electromagnetically Operated Valve Composed of a Teflon Rod and an Iron Core. C_1, C_2, C_3 - Vacuum Valves

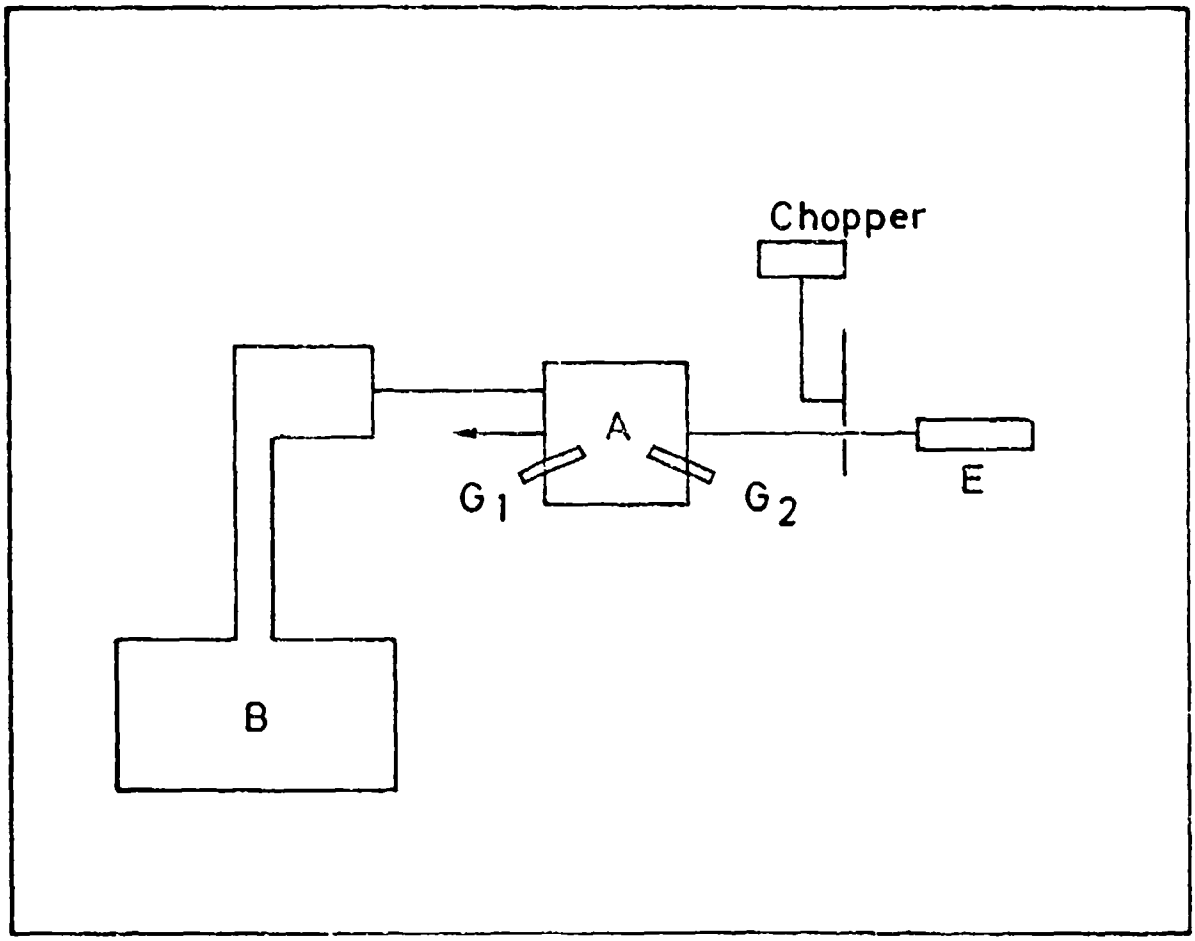

Fig. 31. Block Diagram of the Stereo-Observation System.

P M-6), the light source E was a He-Ne laser (Spectra Physics, Model 134-5, 5 mW), and the time scale device was an electronically stabilized chopper (Ithaco, Model 382). A special problem was posed by the metallic vacuum valves $C_1 - C_3$ which were finally made as shown in Fig. 32.

(1) Calculational Procedure

Due to the stereo-arrangement, the (three dimensional) trajectory and terminal velocity of motion of a solid particle could be calculated unequivocally.

The velocity of fall is given here by (Fig. 33) *

$$|\vec{v}_\omega| = \left\{ v_1^2 + [(v_1^2 \sin^2\alpha_1 + v_2^2 \sin^2\alpha_2 - 2 v_1 v_2 \sin\alpha_1 \sin\alpha_2 \cos \pi/3)/ \sin^2 \pi/3] \sin^2 A_6 \right\}^{1/2} \qquad [57]$$

where $$A_6 = \pi/2 - \sin^{-1}\left\{ [v_1 \sin\alpha_1 / (v_1^2 \sin^2\alpha_1 + v_2^2 \sin^2\alpha_2 - 2 v_1 v_2 \sin\alpha_1 \sin\alpha_2 \cos \pi/3)^{1/2}] \sin \pi/3 \right\} \qquad [58]$$

and v_1, v_2, α_1, α_2 are the magnitudes of the projected velocity and the angles it subtends to the direction of gravity on the optical image plane of the microscope-cameras G_1 and G_2, respectively.

The angle β_1 (Fig. 33) is expressed by

$$\beta_1 = \cos^{-1} (v_1 \cos\alpha_1 / |\vec{v}_\omega|) \quad ; \qquad [59]$$

---

* see Appendix

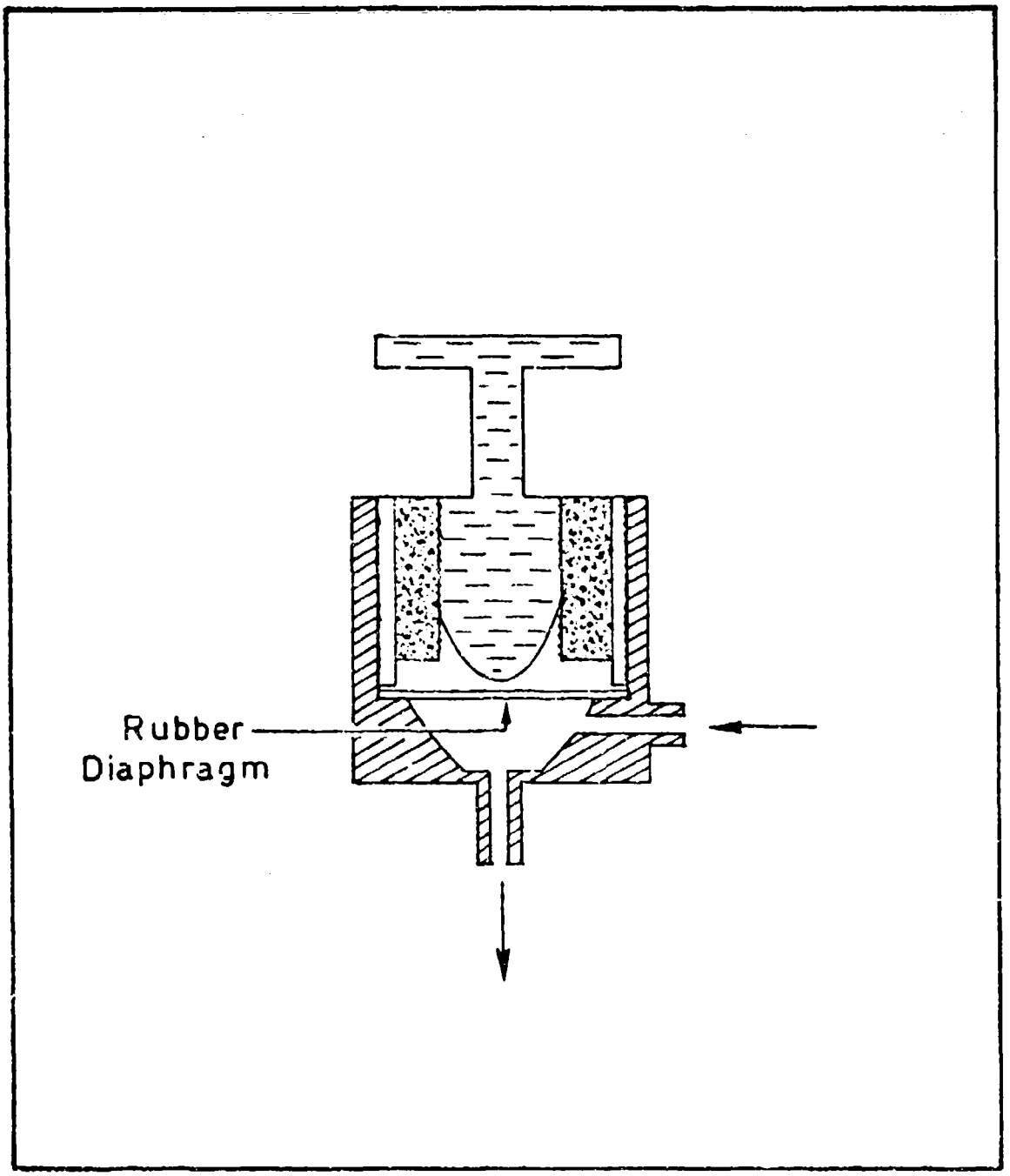

Fig. 32. Schematic Diagram of the Metallic Vacuum Valve.

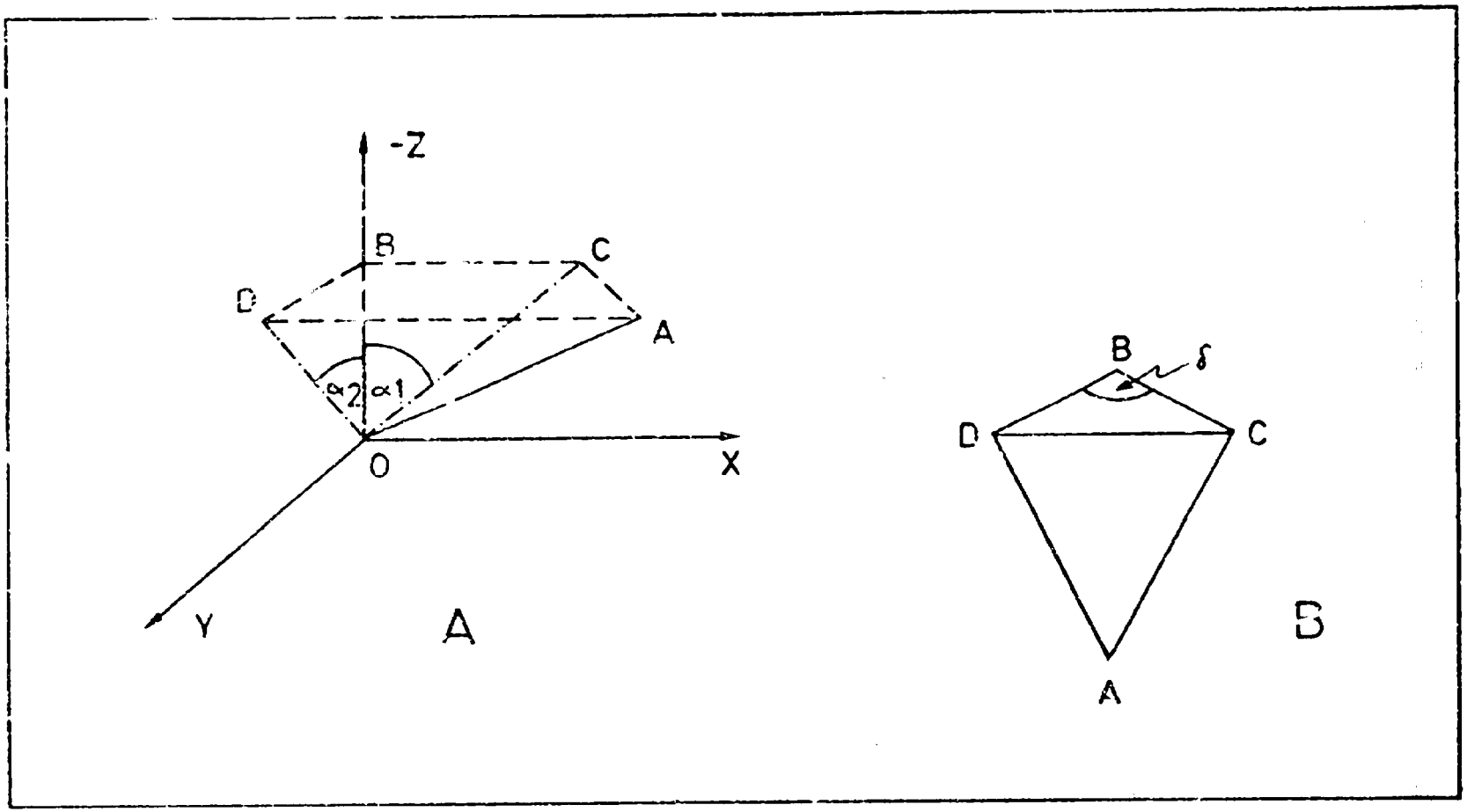

Fig. 33. Trajectory of a Nonspherical Particle in a Fixed Orientation within the Stereo-sedimentation Cell.

A. The Nonorthogonal Coordinate System.

B. A Top View of the Coordinate System.

so, the horizontal and vertical components would be given by

$$(v_x)_\infty = |\vec{v}_\infty| \sin\beta_1 = (|\vec{v}_\infty|^2 - v_1^2 \cos^2\alpha_1)^{1/2} \qquad [60]$$

and

$$(v_z)_\infty = v_1 \cos\alpha_1 \ . \qquad [61]$$

In the case of a cylindrical particle (Fig. 22) which changes its orientation during fall and for a negligible relaxation time after each step (55), one has

$$(\rho/\rho_s)(v_x)_{\infty,1} = (K_1^{-1} - K_3^{-1}) \sin\phi_1 \cos\phi_1 , \qquad [62]$$

$$(\rho/\rho_s)(v_z)_{\infty,1} = K_1^{-1} \sin^2\phi_1 + K_3^{-1} \cos^2\phi_1 , \qquad [63]$$

$$(\rho/\rho_s)(v_x)_{\infty,2} = (K_1^{-1} - K_3^{-1}) \sin\phi_2 \cos\phi_2 , \qquad [64]$$

and

$$(\rho/\rho_s)(v_z)_{\infty,2} = K_1^{-1} \sin^2\phi_2 + K_3^{-1} \cos^2\phi_2 \ . \qquad [65]$$

Thus, denoting $K_1^{-1} = X$, $K_3^{-1} = Y$, $(v_x)_{\infty,1} = A'$, $(v_x)_{\infty,2} = A''$, $(v_z)_{\infty,1} = B'$, $(v_z)_{\infty,2} = B''$, $\sin\phi_1 = x_1$, $\sin\phi_2 = x_2$, $(\rho_s/\rho) = \gamma$, we get from Eqs. [63] and [65]

$$x_1^2 = (B' - \gamma Y)/(X - Y)\gamma \qquad [66A]$$

$$x_2^2 = (B'' - \gamma Y)/(X - Y)\gamma \qquad [66B]$$

which gives on substitution in [62] and [64]

$$(B'-\gamma Y)^{1/2}(\gamma X - B')^{1/2} = A' \qquad [67]$$

and

$$(B''-\gamma Y)^{1/2}(\gamma X - B')^{1/2} = A'' \quad , \qquad [68]$$

or, after squaring and rearranging,

$$\gamma B'(X+Y) - \gamma^2 XY = \alpha' + B'^2 = C' \qquad [69]$$

and

$$\gamma B''(X+Y) - \gamma^2 XY = \alpha'' + B''^2 = C'' \qquad [70]$$

where $A'^2 = \alpha'$, $A''^2 = \alpha''$.

At this stage, designating $\gamma(X+Y) = W$, $\gamma^2 XY = U$,

we obtain from [69], [70]

$$\gamma(X+Y) \equiv W = (C'-C'')/(B'-B'') = \alpha' \qquad [71]$$

and

$$\gamma^2 XY = U = B'\alpha' - C' = c' \quad . \qquad [72]$$

Finally, from Eqs. [71] and [72] we get a quadratic equation for X which can be easily solved. It should be noted that, for the cylindrical case, $K_1 > K_3$, and so $X < Y$.

Experiments with the stereo-sedimentation cell are being carried out now.

VIII. LITERATURE CITED

1. John Happel and Howard Brenner, "Low Reynolds Number Hydrodynamics," Prentice-Hall, 1965, 5.2-5.4.

2. Chandrasekhar, S., Stochastic Problems in Physics and Astronomy, Revs. Mod. Physics 15, 20 (1943).

3. Benarie, Michael, Der Einfluss der Form fester Staubteilchen auf ihre Filtriebarkeit, Staub 23, 50-51 (1963).

4. Davies, C.N., Size, Area, Volume and Weight of Dust Particles, Ann. Occup. Hyg. 3, 219-25 (1961).

5. Medalia, Avrom I., Dynamic Shape Factors of Particles, Powder Technology 4, 117-38 (1970/71).

6. John Happel and Howard Brenner, "Low Reynolds Number Hydrodynamics," Prentice-Hall, 1965, 5.7.

7. John H. Perry, Ed., "Chemical Engineers' Handbook," McGraw-Hill, 1950, Spray Dryers, pp. 839-48.

8. N.A. Fuchs and A.G. Suttugin, "Aerosol Science" (C.N. Davies, Ed.), Academic Press, 1966, Generation and Use of Monodisperse Aerosols, Chap. I, 3.2.

9. N.A. Fuchs and A.G. Suttugin, ibid. Chap I, 3.3; also: N.A. Fuchs, "Assessment of Airborne Particles" (Mercer, Morrow, and Stober, Eds.) Thomas, 1972, Laboratory Powder Disperser, pp. 206-8.

10. N.A. Fuchs and A.G. Suttugin, ibid, Chap. I, 2.2.

11. Pierre St.-Amand, Nucleation by Silver Iodide and Similar Materials, Proceeding Sky-Water Conference, Physics and Chemistry of Nucleation, U.S. Department of Interior, Bureau of Reclamation, Office of Atmospheric Water Resources, Denver, Colorado, pp. 305-46, July 1967.

12. John H. Perry, Ed., "Chemical Engineers' Handbook," McGraw-Hill, 1950, Evaporation from Liquid Drops, pp. 805-7.

13. N.A. Fuchs, "Evaporation and Droplet Growth in Gaseous Media," Pergamon, 1959, Nonstationary Evaporation and Growth of Droplets, pp. 65-6.

14. Reiss, H., The Growth of Uniform Colloidal Suspensions, J. Chem. Phys. 19, 482-7, 1951; also: Y. Boisdron and James R. Brock, "Assessment of Airborne Particles"(Mercer, Morrow, and Stober, Eds.), Thomas, 1972, Particle Growth Processes and Initial Particle Size Distributions, Chap. 7.

15. Brian H. Kaye, "Assessment of Airborne Particles" (Mercer, Morrow, and Stöber, Eds.), Thomas, 1972, Possible Automation Procedure for the Zeiss Ender Particle Size Analyzer, Chap. 12.

16. P. Kotrappa, ibid. Shape Factors for Aerosols of Coal, UO_2, and ThO_2 in Respirable Size Range, Chap. 16.

17. Stöber, W., ibid, Dynamic Shape Factors of Nonspherical Aerosol Particles, Chap. 14, pp. 264-6.

18. Hochrainer, D., A New Centrifuge to Measure the Aerodynamic Diameter of Aerosol Particles in the Submicron Range, J. Coll. Interface Sci. 36, 191-4 (1971).

19. Timbrell, V., "Assessment of Airborne Particles" (Mercer, Morrow, and Stober, Eds.), Thomas, 1972, An Aerosol Spectrometer a.. its Applications, Chap. 15.

20. Gallily, Isaiah, On the Orientation of Nonspherical Particles at Solid Surfaces. A Method of Analysis, J. Coll. Interface Sci., 37, 403-9 (1971)

21. Davis, C.N., Ref. 4.

22. Cartwright, J., Particle Shape Factors, Ann. Occup. Hyg. 5, 1963-71 (1962).

23. Millipore Filter Corporation, Bibliography, May 1964, III Contamination Analysis, p. 19.

24. Walkenhorst, W. Feinste Siebe fur die Quantitative Probenahme von Schwebstoffen zur Elektronenmikroskopischen Auswertung, Staub, 30, 246 (1970).

25. May, K.K., The Cascade Impactor: An Instrument for Sampling Coarse Aerosols, J. Sci. Instrum. 22, 187-95 (1945).

26. Littlefield J.B., and Schrenk, H.H., On the Midget Impinger, U.S. Bur. Mines R.I. No. 3387.

27. Royco Model 200 Particle Counter, Royco Instrument Inc., Melno Park, California.

28. Derjagin, B. and Vlasenko, G., Kolloid. Zhur. 13, 249 (1951).

29. Cadle, R. D., Particle Size Determination, Interscience, 1955 p. 139.

30. Hooper, V. D. and Labby, T. H., The Electronic Charge, Proc. Roy. Soc. London, A 178, 243-72 (1941).

31. Lucien Dautrebande, "Microaerosols," Academic Press, 1962, Production of Liquid and Solid Micromecellar Aerosols, Chap. I , p. 6.

32. Gallily, Isaiah, "Technique for Retarding Evaporation in Gas-Atomization of Solutions and Suspensions," New Technology Transmittal (NT Control Number NPO 11136), JPL, California, January 3, 1969.

33. Espenscheid, W. F., Matijevic, E , and Kerker, M., Aerosol Studies by Light Scattering. III. Preparation and Particle Size Analysis of Sodium Chloride Aerosols of Narrow Size Distribution, J. Phys. Chem. 68, 2831-42 (1964).

34. Hochrainer, D., Private communication, (1971).

35. N.A. Fuchs, "Aerosol Science" (C.N. Davies, Ed.), Academic Press, 1966, Generation and Use of Monodisperse Aerosols, Chap. I , 3.2.

36. Madelaine, G. and Morel, C., Etude des Spheres de Latex Monodispersees par Microscope Electronique et Spectrometer a Diffusion de Lumiere, Ann. Occup. Hyg. 9, 135-47 (1966).

37. Raabe, Otto G., The Dilution of Monodisperse Suspensions for Aerosolization, Am . Ind. Hyg. Assoc. J., pp. 439-43 (September-October, 1968)

38. See Ref. 25 for same principle

39. Shinnar, Reuel and Church, James M., Statistical Theories of Turbulence In Predicting Particle Size in Agitated Dispersions, Ind. Eng. Chemistry 52, 253-56 (1960).

40. Hamaker, H. C., The London-Van der Waals Attraction between Spherical Particles, Physica 4, 1058-72 (1937).

41. Bradley, Stevenson R., The Cohesion between Smoke Particles, Trans. Faraday Soc. 1088-90 (1936).

42. Dube, G. P. and Das Gupta, H. K., Indian J. Phys. 13, 411 (1939).

43. Vold, Marjorie J., Van der Waal's Attraction between Anisometric Particles, J. Coll. Sci. 9, 451-9 (1954).

44. M. Corn, "Aerosol Science" (C. N. Davies, Ed.), Academic Press,1966, Adhesion of Particles, Chap. XI.

45. Wells, O. C., Correction of Errors in Electron Stereomicroscopy, Brit. J. App. Physics 11, 199-201 (1960).

46. H. Lamb, "Hydrodynamics," Dover, 1932, Slow Translation of a Sphere, pp. 597-8.

47. Oseen, C. W., "Neuere Methoden und Ergebnisse in der Hydrodynamik," Leipzig : Akademische Verlag, 1927 (taken from N. A. Fuchs, "The Mechanics of Aerosols," Pergamon, 1964,pp. 37-40).

48. Proudman, I. and Pearson, R. A., Expansions at Small Reynolds Numbers for the Flow Past a Sphere and a Circular Cylinder, J. Fluid Mech. 2, 237-62 (1957).

49. Aoi, T., The Steady Flow of Viscous Fluid Past a Fixed Spheroidal Obstacle at Small Reynolds Numbers, J. Phys. Soc. Jap. 10, 119-29 (1955).

50. H. Lamb, "Hydrodynamics," Dover, 1932, Circular Cylinder, pp. 615-6.

51. Epstein, Paul S., On the Resistance Experienced by Spheres in their Motion through Gases, Phys. Revs. 23, 710-33 (1924).

52. Dahneke, Barton E., Slip Correction Factors for Nonspherical Bodies - II - Free Molecule Flow, J. Aerosol Sci. 4, 147-61 (1973).

53. Dahneke, Barton E., Slip Correction Factors for Nonspherical Bodies. III - The Form of the General Law, J. Aerosol Sci., 4, 163-70 (1973).

54. Oberbeck, H. A., Crelles J. 81, 79 (1876) (taken from Lamb, "Hydrodynamics," Dover, 1932, pp. 604-5).

55. Gallily, Isaiah, On the Drag Experienced by a Spheroidal, Small Particle in Gravitational and Electrostatic Fields, J. Coll. Interface Sci., 36, 325-39 (1971); also, Gallily, Isaiah, ibid., 41, 608 (1972).

56. Davies, C. N., The Sedimentation of Small Suspended Particles, Trans. Inst. Chem. Engrs. Suppl. 25, 25-39 (1947).

57. N. A. Fuchs, "The Mechanics of Aerosols," Pergamon, 1964, p. 245.

58. N. A. Fuchs, ibid., p. 38.

59. Preining, O., The Stokes Diameter of Ellipsoidal Particles, Atmos. Environ. 1, 271-85 (1967).

60. Brenner, H. and Condiff, D.W., Transport Mechanics in Systems of Orientable Particles. III Arbitrary Particles, J. Coll. Interface Sci. 41, 228-74 (1972).

61. John Happel and Howard Brenner, "Low Reynolds Number Hydrodynamics," Prentice-Hall, 1965, pp. 225-6.

62. N.A. Fuchs, "The Mechanics of Aerosols," Pergamon, 1964, p. 26.

63. N.A. Fuchs, ibid., p. 64.

GLOSSARY

a – semi-axis of an ellipsoidal particle

$a_\perp$ – semi-equatorial axis of a spheroidal particle

a' – defined in text

$A_\perp$ – constant defined in text

$A_\parallel$ – instrumental constant, defined in text

A_3, A_4, A_5, A_6 – defined in text

A', A'' – defined in text

b – semi-axis of an ellipsoidal particle

$b_\perp$ – semi-polar axis of a spheroidal particle

b' – defined in text

B – fluid dynamic mobility of an aerosol particle

$B_\perp$ – instrumental constant, defined in text

B', B'' – defined in text

c – semi-axis of an ellipsoidal particle

c' – defined in text

$c_\perp$ – concentration of salt in bulk solution

$\vec{C}_R$ – coupling tensor defined with respect to center of hydrodynamic reaction

C – diameter of a cylindrical particle

C_i, C_j – diameters of image of a cylindrical particle viewed along i, j directions, respectively

$C_\perp, C_\parallel$ – constants defined in text

d – diameter of a spherical particle; d_a – aerodynamic diameter; d_p – projected area diameter; d_s – Stokesian diameter; d_v – volumetric equivalent diameter

d_A, d_B – lateral displacements of sedimented particle from projection of points A and B, respectively

$D_{r,s}$ – rotational diffusion coefficient of a spherical particle

$D_{r,ell}$ – rotational diffusion coefficient of an ellipsoidal particle

$\vec{E}$ – intensity of electrostatic field

$\overline{E_T(\ell_{eff})}$ - relative, kinetic energy of turbulence, expressed in text

E_a - energy of adhesion between aggregate "primaries" separated by $\vec{\ell}_{eff}$.

$f(n,\bar{n})$ - distribution density of agglomerate size

$f(s)$ - distribution density of dried-up salt particles

$\vec{F}$ - force acting on a particle

$F(n)$, $F(n)_{nc}$ - cumulative frequencies, defined in text

$\vec{g}$ - acceleration of gravity; g - absolute value of $\vec{g}$

$g(r)$ - distribution density of suspension droplet sizes

h_1 - correction term for perspective error, defined in text

$h(r)$ - distribution density of solution droplet sizes

h_c - depth of fall of a rotating particle below diaphragm

$\vec{H}_R$ - angular momentum of an aerosol particle with respect to center of hydrodynamic reaction

$\vec{i}, \vec{i}'$ - unit vectors along coordinates x, x', respectively

$\vec{j}, \vec{j}'$ - unit vectors along coordinates y, y', respectively

K - Boltzmann's constant

k_1 - correction term for perspective error, defined in text

$\vec{k}, \vec{k}'$ - unit vector along coordinates z, z', respectively

$\vec{\vec{K}}$ - translation tensor

K_1, K_2, K_3 - principal resistances of a nonspherical particle

Kn - Knudsen number ($= \bar{\ell}/r$, for example)

ℓ - length of a parallelpiped particle

$\vec{\ell}_{eff}$ - effective separation between two neighbouring "primaries" in an aggregate

$\vec{\ell}_j$ - step length of a randomly moving particle during time interval $t_j, t_j + \Delta t_j$

$\bar{\ell}$ - mean free path of gas molecules within the medium

ℓ_1 - correction term for perspective error, defined in text

$\ell_{i,j'}$ - cosine between coordinate axes i and j'

L - length of a cylindrical particle

L_1 - scale of main flow in an agitated, turbulent aerosol

L_2 - distance along optical axis between the first lens of the scanning electron microscope and the surface of the stub

m - mass of an aerosol particle

m_1 - correction term for perspective error, defined in text

M - magnification of scanning electron microscope

M_i, M_j - magnification of scanning electron microscope when viewing along i, j directions respectively

n - number of primary particles in an aggregate

$\bar{n}$ - average number of primary particles in an aggregate

q - electric charge of an aerosol particle

q_1 - number of atoms per unit volume

a - average number of primary particles per unit volume of suspension

r - radius of a spherical particle

r_1, r_2 - limits of size distribution of spherical particles

r_3 - separation between elements of volume in two neighbouring parallelpiped particles

$\vec{r}_4$ - radius vector of a point in a turbulent fluid from origin of a fixed system of coordinates

R - defined in text

R_a, R_b, R_c - radii of spheres having the same resistance as an ellipsoid moving along axes a, b, c, respectively

s - size of a dried-up salt particle

t - time

T - temperature (^{o}K)

$\vec{T}_{R,n}$ - torque of fluid dynamic forces operating on a particle with respect to center of hydrodynamic reaction; $\vec{T}_{R,g}$, $\vec{T}_{R,el}$ - torques due to gravitation and electrostatic forces, respectively

u'', v'', w'' - cartesian coordinates defined in Fig. 12

$\vec{v}$ - translational velocity of an aerosol particle; $\vec{v}_R$ - velocity of center of hydrodynamic reaction; $\vec{v}_{\infty}$ - terminal velocity;

$(v_x)_{\infty}, (v_z)_{\infty}$ - components of terminal velocity along x, z coordinates, respectively

$U = X Y j^{-2}$

v_1, v_2 - volumes of parallelpiped particles

$\vec{V}(\vec{r}_u)$ - velocity of a point in a turbulent fluid relative to a fixed system of coordinates

$\overline{V^2(i_{eH})} = \overline{V^2(\vec{r}_u) - V^2(\vec{r}_u + \vec{\ell}_{eH})}$

w - working distance of the scanning electron microscope

$W = (X + Y)\gamma$

$x_{i,j} (\equiv X_{i,j})$, $y_{i,j} (\equiv Y_{i,j})$, $z_{i,j} (\equiv Z_{i,j})$ - cartesian coordinates of a photogrammetrically measured particle based on the bisector of the angle between direction of sight i and j (Fig. 14)

x_o, y_o, z_o - cartesian coordinates based on substrate surface of a measured particle (Fig. 14)

(x, y, z), (x', y', z') - cartesian coordinates external to a moving particle and along its principal axes of translation, respectively

x'', y'', z'' - cartesian coordinates defined in Fig. 12

$X \equiv 1/K_1$, for a cylindrical particle

$Y \equiv 1/K_3$, for a cylindrical particle

$z_1 = \sin \Phi_1$

$z_2 = \sin \Phi_2$

Greek Letters

α_o - defined in text

$\alpha = (\tan \Psi)^{**}_{t,m} / (\tan \Psi)_{t,m}$

α_1, α_2 - angles between projection of velocity of fall on image planes of microscope-camera G_1, G_2 and direction of gravity, respectively

α', α'' - defined in text

$\beta = \pi - (\sigma_1 + \sigma_2)$

β_1 - angle between axis of cylindrical particle and vertical coordinate ($\equiv$ direction of gravity)

β_o - defined in text

$\gamma_{o,j}$ - defined in text

δ - angle between directions of observation in the stereo-sedimentation cell

ϵ - local energy dissipation rate per unit mass in an agitated aerosol

ξ_1, ξ_2 - dummy variables

η - scale of eddies of Reynolds number 1 in an agitated aerosol

θ - mutual orientation angle between two parallelpiped particles

θ_1 - angle of Brownian rotation

λ - confocal ellipsoidal coordinate

λ_L - London constant

μ - viscosity of gaseous medium

ρ - density of gaseous medium

τ - relaxation time of an aerosol particle

ω_1 - half the angle between two directions of sight in photogrammetric observation

ω_2 - angle between direction of sight which is closest to the stub and its projection on the latter

φ - orientation angle defined in Figs. 16 and 22

ϕ - orientation angle defined in Fig. 16

Ψ - drift angle

$\vec{\omega}$ - angular velocity of a particle

$\vec{\Omega}$ - rotation tensor defined with respect to center of hydrodynamic reaction

Superscripts

* - denotes value of a "slip flow" regime

Subscripts

e - denotes relation to experiment

el - denotes influence of electrostatic forces

ell - denotes relation to ellipsoid

ex - denotes external influence

g - denotes influence of gravity

h - denotes influence of fluid dynamic forces

j - denotes direction of j coordinate; also - an ordinal number in time intervals

m - denotes maximal value

R - denotes relation to center of hydrodynamic reaction

r - denotes relation to a sphere

t - denotes relation to theory

tr - denotes true value of coordinates of a photogrammetrically observed particle

T - denotes relation to turbulence

v - denotes direction of particle's velocity

$1,2$ - relates to projection on image planes of microscope-camera G_1, G_2, respectively

∞ - denotes terminal state

X. APPENDIX

Here, the lengths (OC) and (OD) as well as the angles α_1 and α_2 (Fig. 33 a) are experimentally measured quantities whereas the angle δ is a known constant of the system.

From Fig 33 a one has

$$\cos \beta_2 = (OB)/(OA) = (OC)\cos \alpha_1 /(OA) \qquad [1A]$$

in which (OA) is given by

$$(OA) = [(OC)^2 + (AC)^2]^{1/2} . \qquad [2A]$$

To calculate (AC) we proceed by employing the cosine-law (Fig. 33 b) whereby

$$(CD) = [(BC)^2 + (BD)^2 - 2(BC).(BD)\cos \delta]^{1/2}, \qquad [3A]$$

while $(BC) = (OC)\sin \alpha_1$ and $(BD) = (OD)\sin \alpha_2$. Also, according to the sine-theorem (Fig. 33 b)

$$(BC)/\sin \widehat{BDC} = (CD)/\sin \delta \qquad [4A]$$

and consequently, since $\widehat{ADC} = \pi/2 - \widehat{BDC}$, it is possible to obtain $\widehat{ADC}$. Thus, using again the sine-theorem, one gets

$$(AC) = (CD)\sin \widehat{ADC}/\sin(\pi - \delta), \qquad [5A]$$

the length (OA) , and finally, from Eq. [1A], the angle β_1 .